JGR Biogeosciences

RESEARCH ARTICLE
10.1029/2021JG006321

Key Points:

- Landslides mobilized carbon at a rate of 2.46 ± 0.12 tC km^{-2} yr^{-1} over 55 years in SE Alaska
- Relatively high connectivity (60%) of landslide deposition to stream networks facilitates C export to the ocean or fjords
- Areas with the highest C mobilization rates were areas of moderate landslide frequency in high C density forests

Supporting Information:

Supporting Information may be found in the online version of this article.

Correspondence to:

B. A. Vascik,
brycevascik@gmail.com

Citation:

Vascik, B. A., Booth, A. M., Buma, B., & Berti, M. (2021). Estimated amounts and rates of carbon mobilized by landsliding in old-growth temperate forests of SE Alaska. *Journal of Geophysical Research: Biogeosciences*, *126*, e2021JG006321. https://doi.org/10.1029/2021JG006321

Received 1 MAR 2021
Accepted 1 NOV 2021

Author Contributions:

Conceptualization: Bryce A. Vascik, Adam M. Booth
Data curation: Bryce A. Vascik, Brian Buma
Formal analysis: Bryce A. Vascik, Adam M. Booth
Funding acquisition: Adam M. Booth
Investigation: Bryce A. Vascik
Methodology: Bryce A. Vascik, Adam M. Booth, Brian Buma
Project Administration: Adam M. Booth
Resources: Brian Buma
Software: Bryce A. Vascik, Adam M. Booth, Brian Buma, Matteo Berti
Supervision: Adam M. Booth
Validation: Bryce A. Vascik, Adam M. Booth, Brian Buma
Visualization: Bryce A. Vascik, Adam M. Booth

Estimated Amounts and Rates of Carbon Mobilized by Landsliding in Old-Growth Temperate Forests of SE Alaska

Bryce A. Vascik[1], Adam M. Booth[1], Brian Buma[2], and Matteo Berti[3]

[1]Department of Geology, Portland State University, Portland, OR, USA, [2]Department of Integrative Biology, University of Colorado, Denver, CO, USA, [3]Department of Biological, Geological, and Environmental Sciences, University of Bologna, Bologna, Italy

Abstract Landslides, a forest disturbance, mobilize carbon (C) sequestered in vegetation and soils. Mobilized C is deposited either onto hillslopes or into the water, sequestering C from and releasing C to the atmosphere at different time scales. The C-dense old-growth temperate forests of SE Alaska are a unique location to quantify C mobilization rate by frequent landslides that often evolve into saturated moving masses known as debris flows. In this study, the amount of C mobilized by debris flows over historic time scales was estimated by combining a landslide inventory with maps of modeled biomass and soil carbon. We analyzed SE Alaskan landslides over a 55-year period where a total of 4.69 ± 0.21 MtC was mobilized, an average rate of 2.5 tC km^{-2} yr^{-1}. A single event in August 2015 mobilized 57,651 ± 3,266 tC, an average of 63 tC km^{-2}. Depositional fate was inferred using two methods, a standard stream intersection analysis and a second novel approach using simulated debris flow deposition modeling calibrated to the study area. Approximately 60% of debris flow deposits intersected the stream network (9% into mainstem channels, 91% into small tributaries), consistent with long-term modeled connectivity, suggesting that debris flows are likely to contribute to globally significant amounts of C buried in local fjord sediments. Our results are consistent with an emerging consensus that landslide disturbances that mobilize organic carbon may play an important role in the global carbon cycle over geologic time, with coastal temperate forests being hotspots of potential carbon sequestration.

Plain Language Summary The amount of carbon stored in forests and soils on Earth plays an important role in the global climate by storing carbon away from the atmosphere. Landslides displace carbon in forests, and there is a need for estimating how much carbon is being relocated in heavily forested areas. Our study estimates the amount of carbon removed from hillslopes by landslides in SE Alaska, one of the most carbon-rich forests in the United States, and determines where in the landscape this carbon is being transported. Landslides primarily move carbon to either hillslopes or water, which bury carbon and reduce the rate at which it is transferred to the atmosphere. Over a 55-year period, landslides transported as much as 57% of the amount of carbon that was lost due to logging in the Tongass National Forest between 1954 and 1995. Across the landscape, 60% of the landslides deposit into streams, which increases the chance for carbon to be stored for geologic time scales. These findings agree with previous research showing forest disturbances play an important role in the global carbon cycle that moderates climate over geologic time.

1. Introduction

Landslides occur on sloped terrain around the world, causing fatalities, damaging property, disrupting infrastructure networks, and altering ecosystems (Hovius et al., 1997; Jensen et al., 2009; Restrepo & Walker, 2009). Regional landslide rates are influenced by climatic and tectonic conditions, with wet climates initiating rainfall-induced landslides and tectonically active areas initiating earthquake-triggered landslides. Landslides serve as mechanisms for carbon (C) mobilization in densely forested regions by stripping vegetation and soil from hillslopes. Those materials are deposited elsewhere in the landscape and can be exported to the oceans via river systems (Hilton & West, 2020). If landslide-mobilized carbon is efficiently buried in offshore sediments, landslides may then be an important geologic carbon sink, especially if landslide occurs frequently or with large-magnitude events. The amount and the depositional fate of carbon transported

Writing – original draft: Bryce A. Vascik
Writing – review & editing: Bryce A. Vascik, Adam M. Booth, Brian Buma, Matteo Berti

during landslide triggering events have only been determined for a handful of events around the world (e.g., Clark et al., 2016; Hilton et al., 2011; Madej, 2010; Mohr et al., 2017; West et al., 2011), but is likely comparable in magnitude to weathering-related fluxes traditionally thought to control the carbon cycle over geologic time scales (Hilton & West, 2020).

Globally, terrestrial ecosystems are estimated to contain 2.76×10^{12} tC in the form of biomass carbon (C_{bio}) and soil organic carbon (SOC) (Wang et al., 2010). Carbon is transferred among three major reservoirs on Earth—on land (terrestrial), in water (oceanic), and the air (atmospheric) — and these transfer rates are of great consequence to biogeochemical cycles and subsequently most lifeforms (Falkowski et al., 2000; Melillo et al., 1993). For erosional events that laterally transfer carbon on land, the impact to carbon budgets depends on whether revegetation post-landslide occurs more rapidly than decay and respiration of mobilized C (Berhe et al., 2007). Otherwise, a net loss from the atmospheric carbon pool would result over the relevant decay and revegetation timescales (Ramos Scharrón et al., 2012; Restrepo & Walker, 2009).

Depositional fate, defined here as to where carbon is deposited once mobilized by a landslide, is a primary control on the timescale for sequestration of mobilized carbon, and whether the landslide deposit acts as a source or a sink to the atmospheric carbon pool (Stallard, 1998). We define short-term sequestration of carbon as soil development timescales (up to thousands of years) and long-term sequestration of carbon as rock formation timescales (at least hundreds of thousands of years). Short-term sequestration of landslide-mobilized carbon occurs through the integration of material into the forest soil, resulting in the accumulation of carbon within the soil organic horizon (Currie et al., 2002). Larger fragments of wood, which we refer to as coarse woody debris (CWD) (>10 cm diameter), are typically deposited on the soil surface or buried in the landslide deposit. Existing CWD and living trees that are converted to CWD by landsliding, throughout a forest contain a substantial fraction of the total carbon. CWD represents 21.1% of aboveground carbon stocks within the temperate forests of SE Alaska ($27{,}750 \pm 540$ tC km^{-2}), equating to an amount of $5{,}860 \pm 210$ tC km^{-2} and live trees amount to $21{,}890 \pm 460$ tC km^{-2} (Yatskov et al., 2019). Residence times for carbon sequestered in the soil vary between hundreds of years and several millenniums depending on soil and climatic conditions (Rumpel et al., 2002; Schimel et al., 1994).

There are pathways by which carbon can leave the terrestrial biosphere, with respiration being a primary flux from the terrestrial to the atmospheric pool. Climate and moisture are two major controls on respiration rates, with cold and dry climates such as tundras experiencing mean soil respiration rates of 60 ± 6 tC km^{-2} yr^{-1}, and warm and wet climates such as tropical moist forests experiencing $1{,}260 \pm 57$ tC km^{-2} yr^{-1} (Raich & Schlesinger, 1992). CWD respiration rates have been measured at 21 tC km^{-2} yr^{-1} in temperate deciduous forests (Gough et al., 2007). In wet and warm climates, up to 76% of carbon within CWD can be transferred to the atmosphere (Chambers et al., 2001) whereas cooler and drier climates experience relatively lower respiration rates (Marra & Edmonds, 1994; Progar et al., 2000). Non-respirated carbon is transferred to the soil of the landslide's deposit over years to centuries through leaching, acting as a local carbon sink from the atmosphere (Russell et al., 2015; Wiebe et al., 2014). Debris containing C that becomes buried during landslide inundation is less likely to experience respiration in the atmosphere. Higher precipitation has been correlated with increased production of dissolved organic matter through leaching in leaf litter, CWD, and soils (Hafner et al., 2005). Landslide deposits that allow for more respiration of carbon to the atmosphere than the accumulation of new C on the deposit are designated as localized carbon sources, whereas those that accumulate more new C than is respired are designated carbon sinks with respect to the atmosphere (Ramos Scharrón et al., 2012).

Long-term C sequestration occurs when C is buried below the water table and incorporated into the sedimentary record (Frith et al., 2018; Galy et al., 2007). This is facilitated by direct deposition into a body of water, or to a stream that can efficiently export CWD and particulate organic carbon (POC) (0.22–0.7 μm) to a body of water. CWD within streams is broken down into smaller fragments (POC), allowing fluvial entrainment to become feasible, and fragments are subsequently carried downstream and efficiently exported to larger bodies of water (Triska & Cromack, 1980). This depositional fate also depends on the size of streams landslide deposits into, with smaller streams lacking sufficient stream power to directly export CWD, and POC being transported over longer distances by more intermittent flows, reducing carbon export efficiency. Overall, despite C losses to the atmosphere during stream transport due to metabolization, terrestrial organic matter represents approximately one-third of all buried organic matter within marine

sediments globally and is preferentially remineralized and buried in continental shelf sediments (Burdige, 2005). Carbon burial efficiency increases with a sedimentation rate (Aller, 1998), which causes coastal mountains that exhibit high marine shelf sedimentation due to landslides to be prime locations for the burial of landslide-mobilized carbon, especially when the frequency or magnitude of carbon mobilizing events is high (Frith et al., 2018; Hilton et al., 2011; West et al., 2011).

Of the variety of landslides that exist, debris flows, in particular, may be especially efficient at facilitating the transfer of C to offshore sediments because they have increased mobility relative to other landslide types and typically occur in channels (e.g., Iverson, 1997). Debris flows are moving masses of saturated sediment which often begin as debris avalanches (Varnes, 1958), mobilize into debris flows due to high (near lithostatic) pore-pressures, and entrain soils and aboveground biomass along their runout paths, commonly incising channels down to bedrock (Iverson et al., 1997; Stock & Dietrich, 2006). High rainfall duration and intensity both play a role in the initiation of debris flows (Guzzetti et al., 2008; Segoni et al., 2018). In turn, many regions that experience debris flows are vegetated, such as temperate montane rainforests. Entrained biomass (such as tree trunks, branches, and shrubs) is deposited atop previous landslide deposits, within stream channels, in bodies of standing water, or on alluvial or colluvial fans (Lancaster et al., 2003; May, 2002). As velocity slows due to decreasing slope, acute tributary junction angles, or roughness elements in the runout path, including vegetation, deposition begins and the active flow volume decreases until forming a deposit (Benda & Cundy, 1990; Guthrie et al., 2010; Johnson et al., 2000; Lancaster et al., 2003). Whether inundation occurs in or adjacent to a stream or on colluvial/alluvial fans can influence carbon sequestration rates and timescales. This is largely controlled by valley configuration, as landslides occurring in U-shaped valleys lose momentum before depositing in mainstem channels that have sufficient stream power to export material out of the watershed (Gomi et al., 2004; Johnson et al., 2000).

Predicting debris flow inundation is important due to the hazardous implications of fast-moving debris through settlements (Berti & Simoni, 2007; Cui et al., 2011; Iverson et al., 1998; Reid et al., 2016), as well as predicting where mobilized carbon is deposited. Most methods for predicting debris flow inundation utilize semi-empirical relationships between a debris flow's volume and runout, such as length or inundated planimetric area (Iverson et al., 1998; Reid et al., 2016; Rickenmann, 1999; Scheidl & Rickenmann, 2010). Those semi-empirical relationships are implemented in software such as LAHARZ (Schilling, 1998) or DFLOWZ (Berti & Simoni, 2007).

This study estimates the quantity and depositional fate of C within soils and vegetation mobilized by debris flows in SE Alaska and then compares C mobilization in SE Alaska to other landslide disturbances across the world. Three spatial and temporal dimensions will be examined here (Figure 1): (a) a single storm that occurred in August 2015 near Sitka, AK with a footprint of ~950 km^2, (b) multi-decadal carbon mobilization within the larger (70,586 km^2) Tongass National Forest (TNF) in SE Alaska, and (c) modeled post-glacial (~10 ky) time-scales in a representative small (84 km^2) area containing several watersheds near Sitka. At the two shortest temporal scales, the amount of mobilized carbon is estimated by combining existing maps of landslides and carbon density. The depositional fate of mobilized carbon for all three spatio-temporal scales is determined by estimating the percent of mapped or modeled debris flows which deposited materials on hillslopes versus streams. The modeling used in this study allows us to assess where, throughout the landscape, debris flows are likely to deposit. This is a new approach to infer the fate of mobilized carbon over Holocene time scales and a different application of such runout modeling software.

2. Materials and Methods

2.1. Study Area: Tongass National Forest, Southeast Alaska

2.1.1. Geology

Bedrock of the TNF study area near the Sitka focus area broadly consists of Late Cretaceous mudstones, as well as an older volcaniclastic rock (Gehrels et al., 1994; Kramer et al., 2001). Pleistocene glacial activity has shaped the landscape of the region by carving the bedrock and forming U-shaped valleys, hanging valleys, and fjords (Hamilton & Thorson, 1983; Hamilton, 1994; Kaufman & Manley, 2004). Much of the landscape is within close proximity to either fjords or the Pacific Ocean (Figure 1). West of Sitka rests Mount Edgecumbe, which has erupted basaltic to rhyolitic lava and ash dated to Paleogene and Quaternary periods

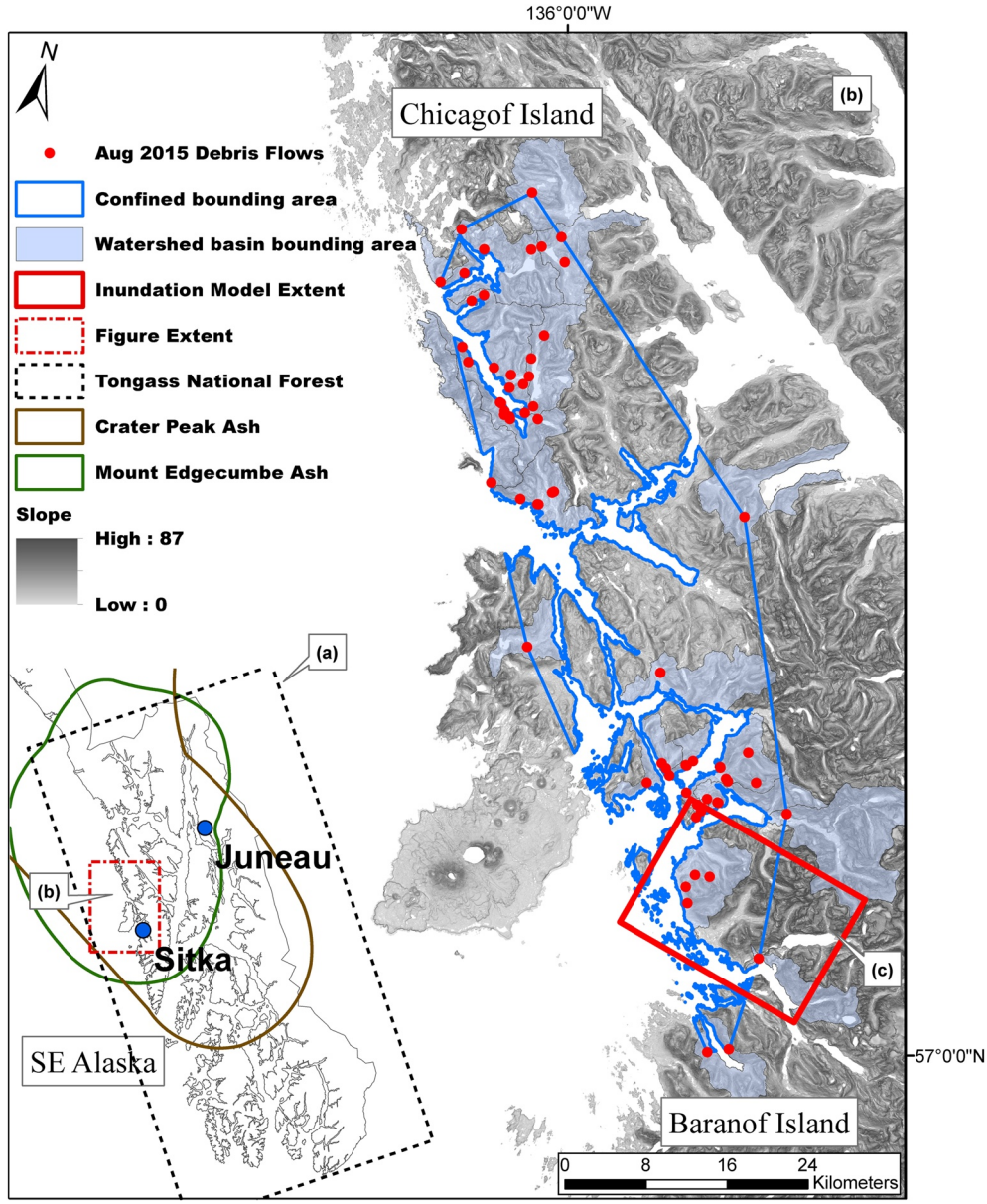

Figure 1. SE Alaska study areas corresponding to the three spatio-temporal scales analyzed in this study. (a) Inset map of SE Alaska, with the spatial extent of (b) indicated by the red dotted line, and the extent of the Tongass National Forest indicated by the dotted black line. Brown polyline represents the extent of Tephra deposited by the 1992 Crater Peak eruption (Neal et al., 1995), green polyline represents the extent of Mount Edgecombe Tephra deposits throughout the Holocene (Riehle et al., 1992). (b) Slope map of study area with debris flows that occurred during a single storm event in August 2015 (red dots). Blue polygons represent an estimate of the "watershed basin" representative area impacted by landsliding delineated by HU-12 watershed boundaries from the National Hydrography Dataset. Blue outline represents an estimate of the "confined" representative area impacted by landsliding using a convex hull. (c) Solid red box represents the extent of the inundation model simulations.

(Gehrels et al., 1994). Soils of the area are shallow and consist of weathered rhyolitic, dacitic, and andesitic ash sourced from Mount Edgecumbe (Riehle et al., 1992) underlain by glacial till. These ash beds are observed to be as thick as 3 m in some locations near Sitka. Glacial deposits are prevalent throughout the region in the form of till, moraine, and outwash sediments and are positioned between volcanic ash and bedrock (Kramer et al., 2001). Both till and ash deposits have low permeability (Schroeder, 1983). Many landslides triggered near Sitka during the 2015 storm failed at the till-ash contact or within the till in the subsurface (Booth et al., 2020; Sitka Geotask Force, 2016). While the thicker ash beds are near Sitka, there are also

regions in SE Alaska with high landslide densities, but little to no ash in the soils (Figure 1). Colluvial soils are present on lower slopes due to mass wasting events occurring after glacial retreat (Schroeder, 1983).

2.1.2. Climate

Southeast Alaska is classified as having a mid-latitude maritime climate with annual precipitation increasing with elevation, starting at 2.2 m yr^{-1} near sea level in Sitka (SNAP, 2018; Wendler et al., 2016). Average high temperatures at sea level are above freezing year-round (Shulski & Wendler, 2007). High winds and intense precipitation are common, often triggering landslides within the region (Johnson et al., 2000; Kramer et al., 2001; Yao et al., 2018). A storm on August 18, 2015 initiated over 60 landslides, many of which mobilized into debris flows (Figure 1). Meteorological data (Horel et al., 2002) reported peak 3-hr rainfall intensity in Sitka at 33 mm hr^{-1}, a return period of 25–50 years, and a storm total of 140 mm rainfall in 6 h at sea level (likely higher at elevation).

2.1.3. Biomass and Soil Organic Carbon Stocks and Fluxes

Temperate rainforests have high carbon densities compared to other forests (Keith et al., 2009). Southeast Alaska contains an estimated 2.8 ± 0.5 Pg C (Leighty et al., 2006), with 1.21–1.52 Pg C in aboveground biomass (Buma & Thompson, 2019) and approximately 1.8 Pg SOC in an area of approximately 70,586 km^2 (McNicol et al., 2019). The montane forests of SE Alaska are mostly undisturbed by human activities and are carbon-dense, estimated to contain 8% of all terrestrial biosphere carbon in the contiguous United States and 0.25% globally (Leighty et al., 2006). Parts of the region have been logged, resulting in a C loss of 60,000–307,000 tC yr^{-1} (0.85–4.35 tC km^{-2} yr^{-1}) from 1900 to 1995 (Leighty et al., 2006), but a majority of land contains old-growth forests (Berg et al., 2014). Carbon flux from the atmosphere to living biomass is approximately 85 tC km^{-2} yr^{-1}, which should be roughly comparable in magnitude to the flux of carbon respired to the atmosphere from soil, assuming equilibrium. This rate is relatively low compared to warmer, tropical climates (Raich & Schlesinger, 1992). SE Alaskan fjords are estimated to bury 0.265 tC km^{-2} yr^{-1}, where the area refers to watershed area draining to the fjord, a rate that is higher than other fjord systems in the world (Smith et al., 2015). For erosional carbon fluxes, a relatively small debris flow with a volume of 1,000 m^3 can entrain hundreds of metric tons of carbon (Booth et al., 2020; Buma & Johnson, 2015), and large storm events can trigger hundreds of debris flows within a single day (Clark et al., 2016; Johnson et al., 2000; Sitka Geotask Force, 2016).

2.1.4. Landslide Inventory

The National Forest Service maintains a landslide inventory for the entire Tongass National Forest, which we used in this study and refer to as the "TNF Landslide Inventory" (Tongass National Forest, 2019). The inventory was derived by aerial photo analysis with photos from as early as 1929 in some areas and is updated approximately annually as a publically available GIS database. The initiation dates of a majority of older landslides within the inventory are estimated between the first time they are seen on a photo and the most recent previous photo taken in that area. Because of limited and irregular aerial photo coverage prior to 1960, the inventory is most complete from the years 1960–2015, and we analyzed only this 55-year time period, which includes the August 2015 Sitka event. For modern storms, aerial photography is often collected shortly after to assess landslide impact, providing high confidence in regards to the occurrence date for landslides initiated. To analyze connectivity and C mobilization for the single August 2015 event, landslides with an initiation date of 18 August 2015 were selected. Our analysis used landslide polygons within the debris flow type categories in the inventory ("Debris avalanche", "Debris torrent", and "Combination debris avalanche and debris torrent") which delineate the initiation, scour, and deposition zones of the landslides from aerial photography. A total of 7,156 landslides fit our criteria, the smallest of which had an area of 40 m^2 while the largest was 199,000 m^2. We note that aerial imagery-based inventories are limited to what is visible from the imagery as field verification is difficult in the study area, and tend to underestimate landslide runout, which can continue into forested areas and can misclassify the landslide type.

2.2. Methods

2.2.1. Carbon Models

Determining the depositional fate of mobilized carbon, the focus of our study is achievable by coupling landslide inventories with maps of C_{bio} and SOC derived from field measurements and remote sensing data (Clark et al., 2016; Frith et al., 2018; Hilton et al., 2011; Wang et al., 2016; West et al., 2011). We utilized two recent and comprehensive datasets which modeled C_{bio} and SOC across SE Alaska. Both datasets were developed using random decision forest algorithms to predict carbon density using environmental and disturbance variables coupled with Forestry Inventory and Analysis (FIA) data across the landscape (Buma & Thompson, 2019; McNicol et al., 2019). FIA plots are located approximately every 5 km throughout the United States, providing detailed data on forest conditions and the amount of aboveground biomass carbon at each plot (Barrett & Christensen, 2011). Random forest algorithms use classification and regression trees to determine significant variables in order to predict the amount of carbon stored in biomass and soil. The dominant variables that predicted C_{bio} were observed forest cover, slope, elevation, and the likelihood of landslide initiation (Buma & Thompson, 2019) and for SOC the dominant variables were elevation, wetness, and slope position (McNicol et al., 2019). Biomass was converted to carbon at the standard rate of 50% (Houghton et al., 1997). The resulting products are C_{bio} and SOC continuous rasters for SE Alaska at resolutions of 30 m (C_{bio}) and 90.5 m (SOC) which we resampled using the nearest neighbor method to 5 m for consistency with an IfSAR-derived digital elevation model (DEM) to allow for finer resolution analysis with landslide polygons (U.S. Geological Survey, 2017).

An observed versus predicted fit r^2 value of 0.69 for biomass in FIA plots was reported by Buma and Thompson (2019). The biomass model included a lower and upper carbon estimate which reflects different scaling factors to accommodate underestimation of aboveground biomass calculated in FIA forest plots as identified by Leighty et al. (2006). In this study, we compute mobilized C_{bio} for both the lower and upper biomass models and report the average, with the range as uncertainty. SOC estimated by McNicol et al. (2019) had a predicted versus observed r^2 value of 0.73 and RMSE of 11,900 tC km^{-2}, indicating that, like the C_{bio} model, the SOC model reasonably predicts carbon across the landscape. Our final uncertainty on mobilized C includes the difference between the C_{bio} models and the RMSE for the SOC model added in quadrature.

2.2.2. Representative Total Area Afflicted by Landsliding

For the 2015 event, two methods were used to delineate spatial extents of landsliding (Figure 1). A "watershed basin" bounding area of 790 km^2 was defined as the combined area of individual USGS National Hydrography 12-digit hydrologic units, which typically encompass 4,046–16,187 hectares (U.S. Geological Survey, 2018), that contained landslides used in our analysis. Watersheds that did not have any landslides initiated within them were not included in the "watershed basin" area. A "confined" bounding area of 1,103 km^2 was established via a convex hull boundary which encompasses locations for the 2015 landslides. For both spatial extents, areas containing water (fjords, ocean, etc.) were excluded to only account for land affected by landsliding.

2.2.3. Spatial Distribution of Mobilized C in the TNF

To visualize broad spatial patterns in C mobilization, a quartic kernel density function (Silverman, 1986), which smooths data points to calculate magnitude-per-area, was applied to the sum of SOC and C_{bio} distributions (tC km^{-2}), landslide occurrences km^{-2} (n = 7,156), and mobilized C_{bio} (tC km^{-2}) with a window size of 5 km and a cell size of 25 m over the entire TNF. This highlights the broad distribution and magnitude of landslides and C throughout the landscape without being overly sensitive to specific, individual landslides.

2.2.4. Long-Term Debris Flow Inundation Modeling

Since the analysis of the TNF Landslide Inventory offers a relatively short window of time compared to the timescales associated with carbon sequestration and respiration, we use empirical runout modeling in a Monte Carlo framework to estimate the longer-term spatial pattern of debris flow deposition for a representative area on northern Baranof Island (Figure 1). Debris flow initiation locations were first chosen by thresholding an existing susceptibility map (Buma & Johnson, 2015), and a volume associated with each initiation site was selected randomly from a log-normal distribution based on data from Booth et al. (2020). We then used the DFLOWZ inundation model, which is well-suited to simulating deposition of debris flows

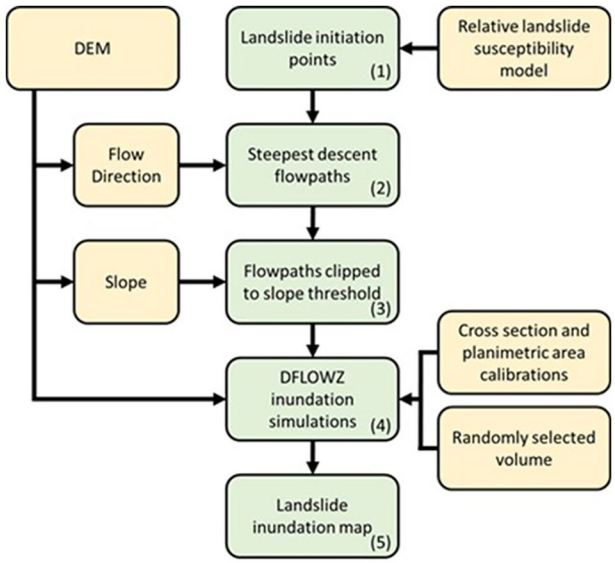

Figure 2. Flow chart describing steps taken (green boxes) and data needed (yellow boxes) for long-term inundation model. Numbers correspond to major steps shown in Figure 3.

in confined channels and on unconfined hillslopes or fans (Berti & Simoni, 2007), to predict each deposit extent (Figure 2). The goal of these simulations was to produce a map of the long-term relative likelihood of debris flow deposition and estimate the average likelihood of deposits terminating in stream channels. Debris flows previously measured in the field to calibrate the model were mainly in undisturbed forests (Booth et al., 2020).

2.2.5. Initiation Points and Volumes

For each simulated debris flow, DFLOWZ requires the location where deposition begins, the volume of the debris flow, a pathway which the debris flow would follow, and coefficients that quantify deposit geometry for calibrating depositional behavior. To establish where landslide initiation occurs, we used a relative landslide initiation susceptibility model for SE Alaska developed using a generalized linear model (Buma & Johnson, 2015). In that study, landslides mapped by the Tongass National Forest Service were analyzed for initiation site characteristics to produce a continuous model of relative initiation susceptibility at locations across the landscape. Significant variables used to model susceptibility were contributing area, slope, soil type, exposure to wind, and two topographic indices. Four 2015 landslides occurred within the inundation modeling study area (Figure 1), initiating in zones with relative susceptibility values ranging from 0.09 to 0.19. We, therefore, selected all pixels with relative susceptibility values greater than 0.09 as one set of locations for simulated landslide initiation (Figure 3a). To capture the tendency for areas with higher relative susceptibilities to likely produce more landslides over time, we added a second set of initiation points that exceeded a higher threshold of 0.19. In total, 28,089 points met the lower threshold, and an additional 8,171 points met the higher threshold, which was all processed for debris flow runout for a total of 36,260 simulations. Results for the inundation simulations represent a rough estimation of the Holocene timescale of landsliding on northern Baranof Island, assuming a background rate of 113 debris flows per century in the model domain, as documented in nearby Haida Gwaii (Barth et al., 2020). Each initiation point was assigned a random volume selected from a log-normal distribution (mean = 2,830 m^3, sd = 6,190 m^3) produced from field measurements near Sitka (Booth et al., 2020).

2.2.6. Steepest Descent Flowpaths

The steepest descent flowpath from each initiation point was defined using the D8 flow direction algorithm (O'Callaghan & Mark, 1984) on a 5 m resolution DEM derived from IfSAR data and publically available from the 3DEP USGS program (U.S. Geological Survey, 2017; Figure 3b). The resulting flowpath represents the path by which a landslide would likely travel if initiated at the input point. A slope map derived from the 5 m DEM was used to clip flowpaths to include only the depositional zone of a hypothetical debris flow from the respective initiation point. To do so, slope values were attached to vertex points from the steepest descent polylines. If a vertex slope value decreased below an approximate maximum depositional threshold for SE Alaskan debris flows (20°) (Booth et al., 2020; Johnson et al., 2000), for more than two vertices in a row, the polyline above those vertices was removed. The resulting clipped polylines represent the flowpaths for debris flow deposition only and were subsequently fed into the DFLOWZ program to be processed for inundation prediction (Figure 3c). The model does not incorporate landscape evolution over time, despite debris flows being a major contributing factor to hillslope erosion (Eaton et al., 2003; Hovius et al., 1997). As a result, our inundation model likely underestimates the extent of debris flow deposition by not accounting for the rerouting of subsequent debris flows around previous deposits. We, therefore, smoothed the final inundation map with a Gaussian filter to highlight broader spatial scale patterns (Section 2.2.7).

2.2.7. DFLOWZ Inundation Simulations

Inundation is predicted using semi-empirical relationships between debris flow volume and the inundated cross-sectional and planimetric areas of a debris flow deposit. We refer to these relationships as "VAB

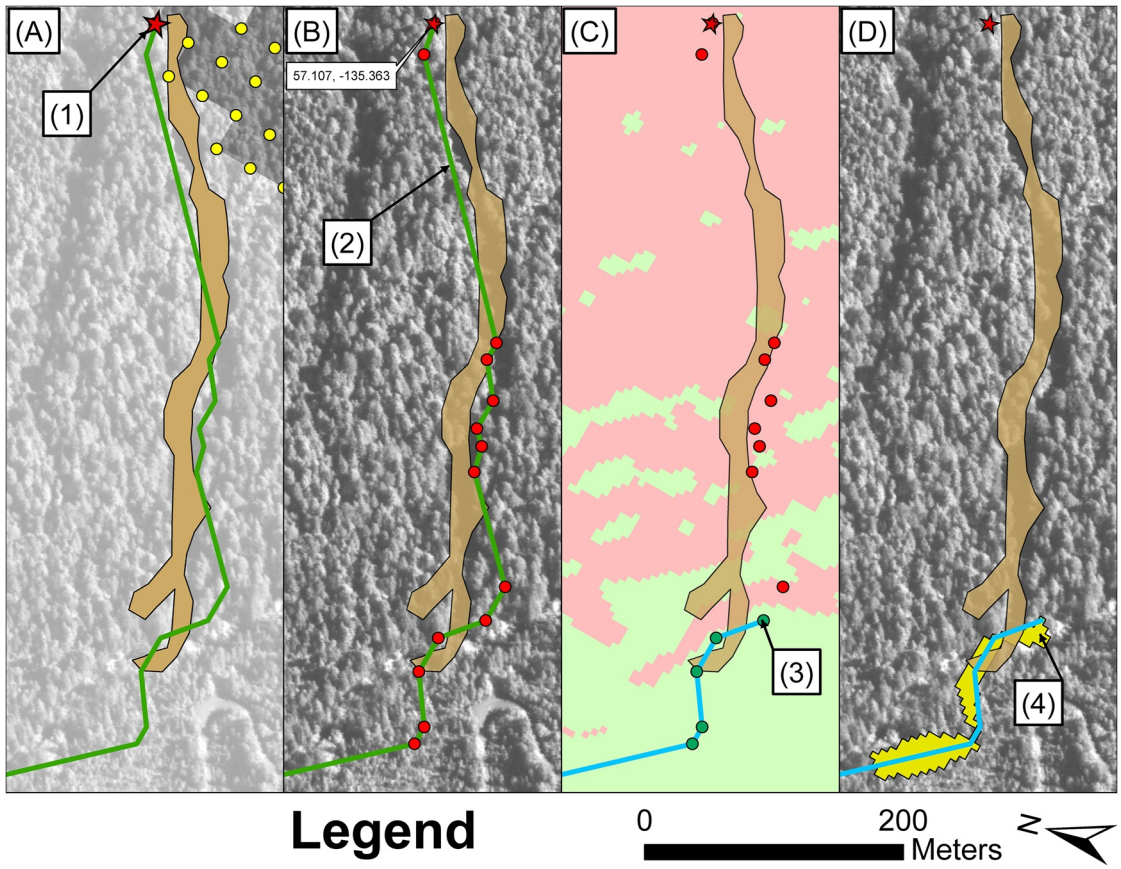
(A)
(B)
(C)
(D)
(1)
(2)
(3)
(4)
57.107, -135.363
Legend
0
200
Meters
N
LS 12313 initiation
LS 12313
Initiation points
DFLOWZ output
DFLOWZ output
Flowpath vertices
Slope
0 - 20
Slope threshold vertices
20 - 78
Relative initiation susceptability
Debris flow flowpath
0.00 - 0.09
0.09 - 0.84
Inundation flowpath

Figure 3.

equations" in this paper. The cross-sectional inundation area of the channel directly above the deposit is estimated by

$$A = aV^{2/3} \quad (1)$$

where A is a cross-sectional area inundated, V is debris flow volume, and a is a mobility coefficient. Similarly, the planimetric area of the deposit is estimated by

$$B = bV^{2/3} \quad (2)$$

where B is inundated planimetric area, and b is another mobility coefficient. The a and b mobility coefficients in Equations 1 and 2 change according to debris flow characteristics such as grain-size, water content, and the presence of coarse woody debris (Booth et al., 2020; Crosta et al., 2003). We use values of $a = 0.11$ and $b = 8$ for the mobility coefficients for this study, which have been calibrated for debris flows in SE Alaska (Booth et al., 2020). These values differ from those of more mobile debris flows, such as fine-grained lahars in the Pacific Northwest, and debris flows in the Italian Alps (Berti & Simoni, 2007; Iverson et al., 1998).

2.2.8. Landslide Inundation Map

To map the spatial extent of deposition for each simulated debris flow with DFLOWZ, cross-sections were established every 40 m along the flow path (as defined in Section 2.2.2) normal to the input flow direction polyline. These cross sections were then "filled" to a level such that the inundated cross-sectional area corresponded to the simulated debris flow volume according to Equation 1. Filling of the cross-sections proceeded down the flow path until the planform area of the deposit was predicted by Equation 2 was reached (Figure 3d). We repeated this process in a semi-Monte Carlo approach for each polyline developed from each initiation point and each randomly selected volume (Section 3.2.1). The final debris flow deposit inundation map is the sum of the number of times each cell in the DEM was inundated by a simulated debris flow (Figure 4a). A 50 m Gaussian filter was then applied to more generally highlight areas of depositional "hotspots" from the resulting inundation simulations while smoothing the abrupt edges of the DFLOWZ results (Section 2.2.5).

2.2.9. Stream Connectivity

Stream deposition was defined as a landslide deposit intersecting a stream network, which we defined using a gradient-slope landscape analysis of the 5 m IfSAR DEM of Baranof and Chicagof Islands (Li et al., 2016; Tarboton et al., 1991). Specifically, a threshold of 16,000 m^2 flow accumulation was visually determined by locating the break-in-slope of a gradient versus drainage area plot indicative of the fluvially-dominated part of the landscape.

A 10-m buffer was applied to the modeled stream polylines to account for possible lateral movement of streams within valleys as well as differences in mapping scale, resolution, and geospatial alignment of the DEM and aerial photo-based landslide inventory (Figure 4). Stream widths in the region are not constant, therefore the 10-m buffer is a compromise between high and low order streams. Deposits from the TNF Landslide Inventory that intersect the stream network were then separated from the total dataset and classified as stream deposits. Within Baranof and Chicagof Islands where streams were modeled, a total of 675 landslides were analyzed for connectivity. The most likely section of a debris flow to intersect with a stream

Figure 3. Example showing steps taken to model landslide inundation across northern Baranof Island. Numbers correspond to steps in the flowchart (Figure 2). Brown polygon is a 2015 debris flow from the Tongass National Forest landslide inventory (LS #12313) near Sitka. (a) Background shading shows relative landslide initiation susceptibility raster with dark cells representing areas greater than the minimum initiation threshold for landslides that occurred during the 2015 storm and light cells representing areas that did not meet the threshold. Yellow points are locations that met the threshold and were processed for landslide inundation. Red star indicates the cell where landslide #12313 was initiated, with a green polyline showing the debris flow steepest decent path. (b) Red points are flowpath polyline vertices of the steepest descent path. (c) Green points are polyline vertices below the 20° slope threshold for landslide deposition, and red points are above that threshold. Blue polyline reconstructed from vertices below 20° represents the flowpath for landslide deposition. (d) DFLOWZ output for the depicted flowpath using a field-measured volume of 6,043 m^3.

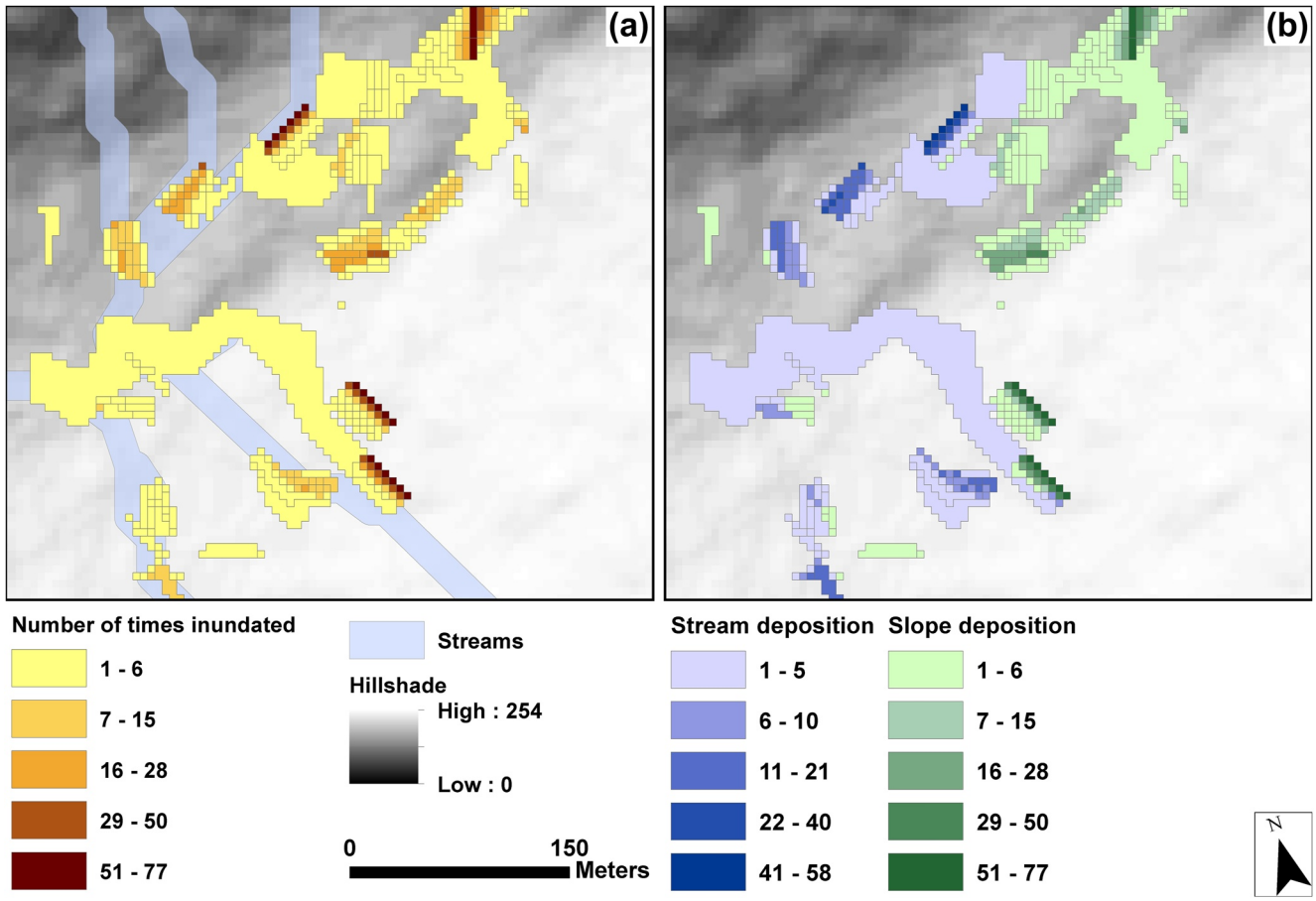

Figure 4. (a) Example of inundation model results shown as individual landslide polygons with colors representing number of times each pixel was inundated, and the buffered stream network in blue. (b) Inundation results split between slope deposits (green color scale) and stream deposits (blue color scale). The location is shown in Figure 6.

is the debris flow snout, where woody debris tends to coalesce due to kinetic sieving (Iverson, 1997). Due to this, we consider any intersection between a debris flow and stream to be a stream deposit but recognize that not all of the mobilized material ends up in the stream. For the TNF dataset, we defined connectivity as the total number of stream deposits divided by the total number of all deposits. Connectivity for the long-term runout model is defined as the number of times stream cells are inundated divided by the total number of times all cells are inundated (Figure 4b). Stream order was modeled using Strahler's methods to determine the amount of connected landslides in smaller streams (1–3 order) and mainstem streams (4–7 order) (Strahler, 1957).

2.3. Carbon Disturbance Compilation

To place SE Alaskan C mobilization in a global context, we compiled studies that estimated C mobilization amounts and rates due to landsliding from five additional forested sites around the world (Figure 7): Redwood Creek, California (Madej, 2010), the New Zealand Southern Alps (Hilton et al., 2011), Taiwan (West et al., 2011), Guatemala (Ramos Scharrón et al., 2012), and the Peruvian Andes (Clark et al., 2016). These studies were selected based on the criteria that they used the same methods as our study–combining landslide inventories with maps of the spatial distribution of C–and reported landslide and carbon densities and rates, which allows for a direct comparison. Although only a few such studies exist, they span a range of forest types from tropical to temperate and a range of landslide triggering events from relatively small storms to large typhoons/hurricanes, which likely captures much of the variance in global landslide C mobilization rates.

3. Results

3.1. 2015 Single Storm Event Carbon Mobilization

The 66 landslides triggered in the August 2015 storm totaled 0.815 km^2 in area and occurred within a footprint of ~947 km^2, giving a landslide density of 0.1%. The mean landslide size was 12,400 m^2, with a range of 300 m^2 to 121,400 m^2. We estimate a total of 57,651 ± 3,266 tC was mobilized by those landslides resulting in landslides mobilizing 70,672 ± 4,004 tC km^{-2} of the landslide area. Using approximations of the "confined" area (1,103 km^2) and "watershed basin" area (790 km^2) affected by the storm (Figure 1) results in 52 ± 3.0 to 73 ± 4.1 tC km^{-2} mobilized within the event "footprint" on Baranof and Chicagof Islands.

3.2. Century-Scale Carbon Mobilization

The TNF Landslide Inventory from 1960 to 2015 contains 7,156 landslides with a total area of 63.8 km^2. The average landslide size is 8,774 m^2 with a range of 40 m^2 to 1,046,023 m^2. Mobilized carbon via landslide based on was 4.69 ± 0.21 MtC over the entirety of the TNF (70,586 km^2). This equates to 66.42 ± 2.9 tC km^{-2} with an annual rate of 1.21 ± 0.05 tC km^{-2} yr^{-1}. Mobilized C_{bio} averaged 36,557 ± 16,157 tC km^{-2} (mean ± standard deviation) of the landslide area, while SOC averaged 41,084 ± 9,673 tC km^{-2} (mean ± standard deviation) of the landslide area, based on the total amount of carbon mobilized over the 55-year time period normalized by total landslide area over the same period.

Using Baranof Island (area of 4,731 km^2) where Sitka is located, we compute a separate C mobilization rate with reduced observation bias that comes to a higher rate of 2.46 ± 0.12 tC km^{-2} yr^{-1}. The 2015 storm represents approximately 1.2% of the total estimated carbon mobilized for the past 55 years within the TNF, which is about two-thirds of the annual C mobilized by landslides in an average year.

3.3. Spatial Distribution of Mobilized C in TNF

The main driver for C mobilization across the region is moderate landslide densities occurring in high carbon areas, instead of reflecting the spatial pattern of landslide density or C density alone (Figure 5). For example, the highest C mobilization densities tend to occur along the west coastline of the study area, where landslide density is moderate, and C density is high (Figure 5). Furthermore, the 70,672 ± 4,004 tC km^{-2} mobilized by landslides during the 2015 storm is higher than the landscape-wide average carbon density of 40,000 tC km^{-2} in the TNF (Leighty et al., 2006). In contrast, the regions with the highest landslide densities, for example, >6 landslides per km^{-2} in the south-central part of the study area, correspond to moderate C mobilization, and regions with high C densities, but few landslides, have low C mobilization densities. Landslides primarily occurred on S-SW facing slopes, coinciding with regional wind storms coming from southerly directions (Buma & Johnson, 2015; Harris, 1989), with an initiating elevation of 337 ± 163 meters (mean ± sd).

3.4. Long-Term Depositional Fate of Mobilized C

Debris flow simulations across northern Baranof Island also indicate mobilized carbon 'hotspots' throughout the landscape (Figure 6). These hotspot locations experienced repeated inundation in the semi-Monte Carlo simulations. Deposition hotspots are generally located in low order channels cut into colluvial slopes below steep valley sidewalls in wide valleys, such as the Indian River valley, or in high order, main stem channels in the narrower valleys, such as Granite Creek and Cascade Creek. These areas are generally located downslope of areas with high initiation susceptibility in broadly convergent topography, so that debris flows originating at multiple sites are routed to a common deposition area. Valley geometry therefore greatly influences whether landslides deposit into streams or not, as well as what order those streams are, with narrow valleys such as Granite Creek and Cascade Creek having a majority of the landslides connected to the main stem, high order stream network, and wide, U-shaped glacial valleys such as Indian River valley having few landslides directly connected to main stem streams.

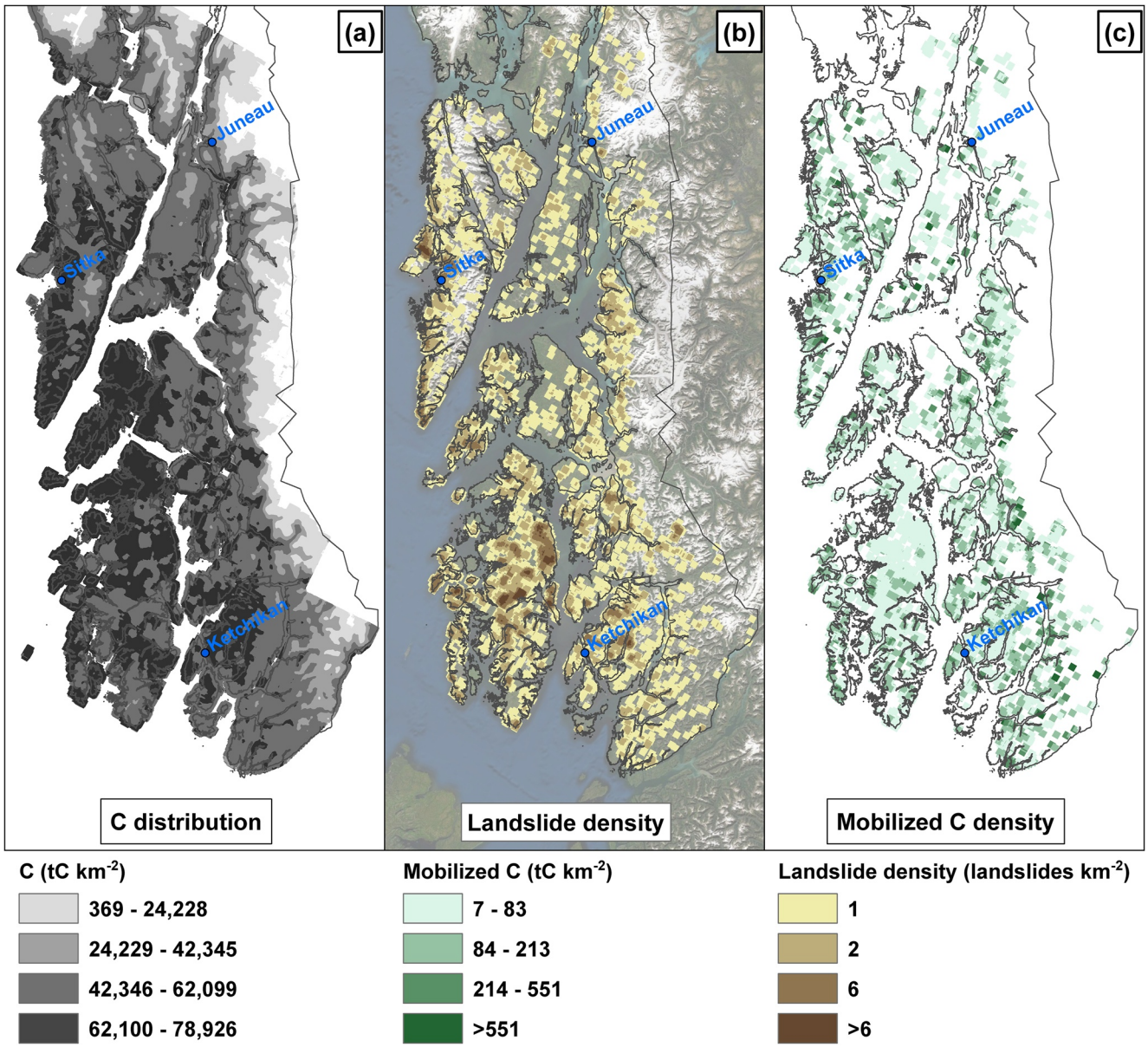

Figure 5. Spatial patterns of (a) Summed soil organic carbon and C_{bio} (average of two endmember C models from Buma & Thompson, 2019), (b) Landslide density overlaying satellite imagery, and (c) Mobilized C_{bio}, smoothed with a moving average quartic kernel with a window size of 5 km. Map extent of Figure 1a.

3.5. Connectivity Analysis

Approximately 71.2% of the 66 debris flows triggered by the 2015 event were classified as stream deposits, with the remaining 28.8% of deposits classified as occurring on hillslopes. An analysis of the simulated debris flows inundation areas on northern Baranof Island resulted in 78.9% of the total inundated cells classified as stream deposits, with the remaining as hillslope deposition at 21.1%. These values are slightly higher but broadly similar to the total TNF landslide connectivity rate, which came to 60.1% stream deposits and 39.9% hillslope deposits. Of the stream deposited landslides, 91% deposited near smaller streams, and 9% near mainstem streams, influencing the depositional fate of the mobilized carbon. For the remainder of our analysis, we opt to use the TNF landslide connectivity rate, as it analyzed a larger area, and the magnitude is similar to the two other connectivity rates.

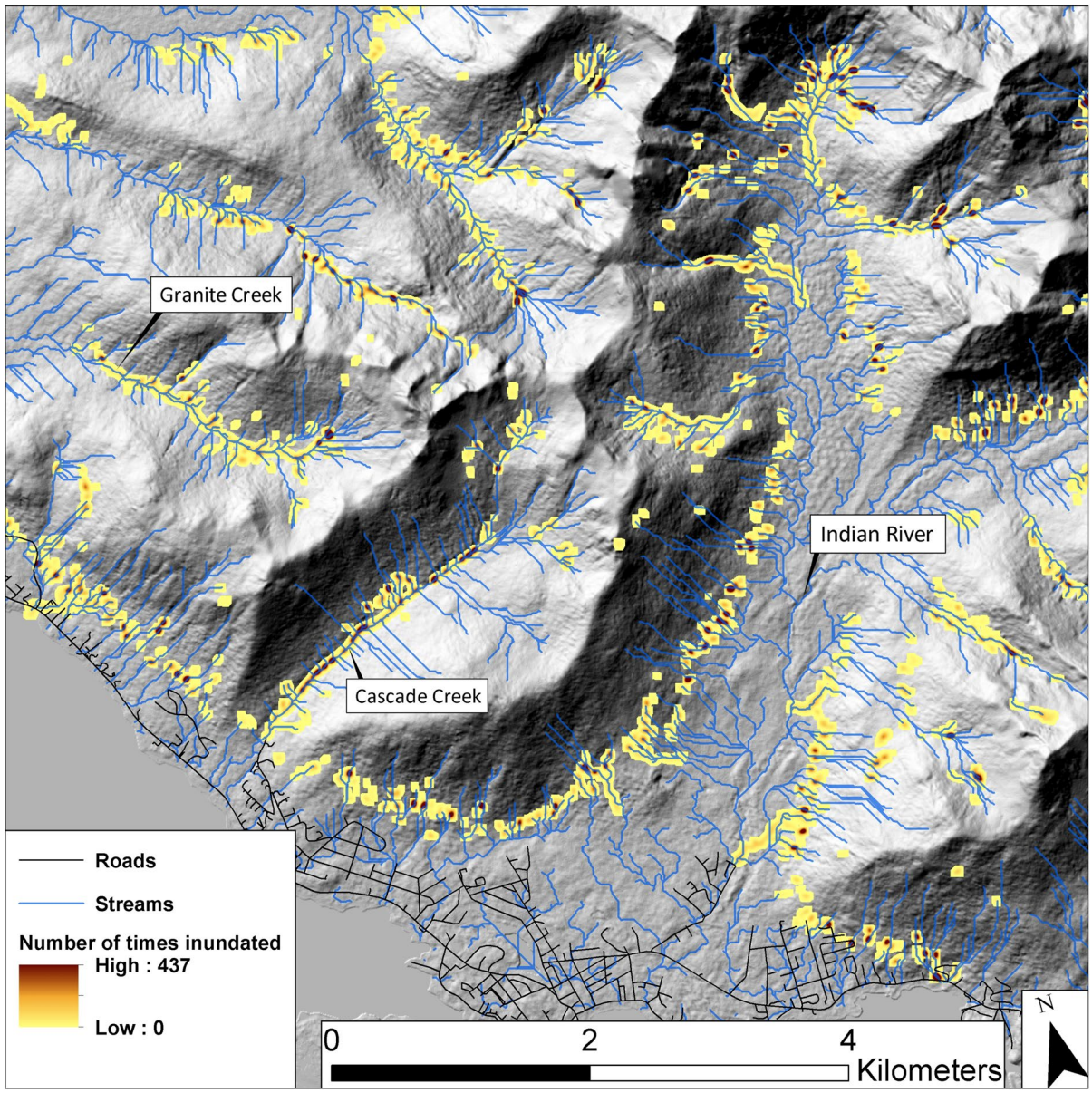

Figure 6. DFLOWZ simulation results smoothed by a 50 m Gaussian filter overlaying a hillshade produced by 5 m IFSAR digital elevation model. Sitka road network indicated by black lines, and blue lines represent the stream network. The blue box indicates spatial extent for Figure 4, and the extent of the entire figure is shown in Figure 1.

The landslide connectivity rate across the SE Alaskan landscape allows us to infer the likelihood of long-term sequestration of mobilized carbon. Due to streams meandering through floodplains, we consider these estimates to be a minimum. Of the 4.69 ± 0.21 MtC mobilized throughout the TNF over the 55-year period, 2.82 ± 0.13 MtC (60.1%) are estimated to have deposited to streams, where carbon can be metabolized, broken down into smaller particulate organic carbon (POC), or directly entrained by discharge and transported to water bodies for long-term sequestration. Of the stream deposited carbon, 2.56 ± 0.12 MtC (91%) deposited in smaller streams and 0.26 ± 0.01 MtC (9%) deposited in mainstem streams. Residence times for POC in streams flowing through temperate forests in the Pacific Northwest have been estimated to be a few hundred years, indicating that although C metabolism does occur during stream transport, POC can be efficiently exported out of watersheds (Goñi et al., 2013). Conversely, the estimated C deposited on slopes equates to $1.87 \pm 0.08 * 10^6$ tC (39.9%), resulting in the burial of mobilized C into the soil horizons, leaching carbon and nutrients to the soil horizon (Hafner et al., 2005), or respiration CO_2 to the atmosphere.

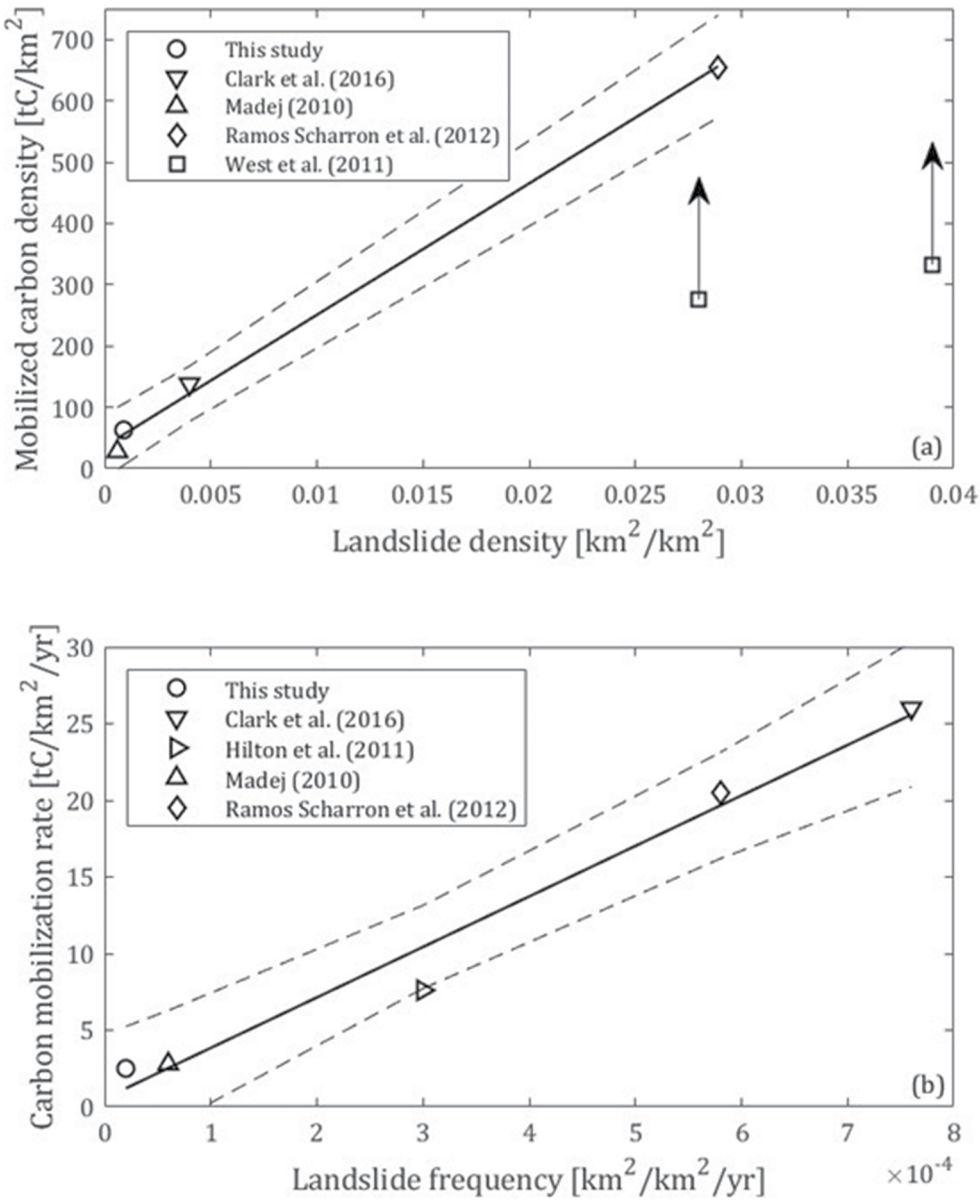

Figure 7. (a) Landslide mobilized carbon density versus landslide density for individual precipitation events. Squares with upward pointing arrows indicate minimum mobilized carbon densities from West et al. (2011), which included only large wood (converted to C at the rate of 48.1%), and were not used in the linear regression. (b) Carbon mobilization rate versus landslide frequency for multiple events (Clark et al., 2016; Hilton et al., 2011) or the assumed recurrence interval for individual events (Madej, 2010; Ramos Scharrón et al., 2012). Solid and dashed lines in both (a) and (b) are linear fits and 95% confidence intervals, respectively.

4. Discussion

4.1. Estimated C Mobilization Rates and Comparison

Taken into context, our estimated total of 57,651 ± 3,266 tC mobilized by the 2015 storm event near Sitka represents less than 0.01% of all carbon sequestered in SE Alaska. However, storm events that trigger debris flows are common in SE Alaska (Johnson et al., 2000; Sidle, 1988), allowing the opportunity for C mobilization to occur regularly in the TNF. Using a return period of 25–50 years for storm frequency, we roughly estimate the C mobilization rate of a storm of this magnitude to be 1,153 ± 65 to 2,306 ± 130 tC yr^{-1} (Horel et al., 2002).

For the 1960–2015 time period, we used the best available data on landslides and C distribution to calculate C mobilization densities and rates, but the incompleteness of the landslide inventory likely caused an underestimation of those values. The TNF Landslide Inventory mapping effort, which is based on air photos and satellite imagery, is only as accurate as of the available data, which often is concentrated near populated areas of the region. Specifically, historic landslides may be missed in the landslide inventory due to expeditious revegetation rates and low-resolution or incomplete historic aerial photography. The smallest mapped landslide within the inventory that mobilized C had an area of 40 m^2 ($4*10^{-3}$ ha) and mobilized 2.2 tC. However, it would take 209,500 landslides of this size to change our estimate of mobilized C by 10%, suggesting that the bias due to small landslides missing from the inventory did not substantially affect our overall results. Landslides that occurred in low C density regions, such as the above treeline, brought the mobilization rate down compared to the representative rate of C mobilization in forested areas throughout the TNF. Additional aerial LiDAR scanning and high-resolution air photos of the entirety of SE Alaska would greatly improve landslide mapping efforts as well as the understanding of revegetation rates for disturbed forests.

Our estimated C mobilization amount for the 2015 storm event and the 55-year historic mobilization rate within the TNF is relatively low in comparison to the other studies included in our compilation (Figure 7). In that compilation, the amount of C mobilized in an individual event (storm, typhoon, or hurricane) ranged from 28 to 6,654 tC km^{-2}, and decadal timescale C mobilization rates varied from 2.5 to 26 tC km^{-2} yr^{-1}. Average C densities of soil and biomass varied by only a factor of two from site to site, from about 23,000 tC km^{-2} (Guatemala; Ramos Scharrón et al., 2012) to about 40,000 tC km^{-2} (TNF; Leighty et al., 2006), which did not explain the order of magnitude range in C mobilization amounts and rates. Instead, landslide density, defined as the ratio of landslide area to the total area affected by an individual event, and landslide frequency, defined as landslide density per time, were significantly positively correlated with C mobilization amount ($r^2 = 0.997$) and rate ($r^2 = 0.977$), respectively (Figure 7). Therefore, although C density in the TNF is higher than in the other regions, that does not make up for the relatively low landslide density and frequency, which were more than an order of magnitude lower than the highest values in the compilation.

One reason for relatively low C mobilization in the TNF is our focus on landslides of only the debris flow class, in order to maintain consistency with inundation simulations using DFLOWZ. Other landslide types (e.g., bedrock landslides) and related mass movements (e.g., snow avalanches) are less frequent but do occur in SE Alaska and have the potential to mobilize carbon (Korup & Rixen, 2014).

Another reason our C mobilization rate is likely an underestimate of the true longer term rate is that several active faults exist in SE Alaska, which could generate earthquakes that trigger landslides, but no earthquake-triggered landslides have occurred historically in the TNF (Doser et al., 1997). In a similar setting (Haida Gwaii, British Columbia), a magnitude 7.8 earthquake in 2012 caused a 13-fold increase in the annual landslide rate in the year of the earthquake (Barth et al., 2020). The earthquake-triggered landslide density there was 0.3%, about threefold higher than that of the 2015 Sitka storm-triggered landslides, while earthquake-triggered landslide densities more generally can be as high as several percent (e.g., Li et al., 2014). Therefore, beyond the historic record, which includes no earthquake-triggered landslides in SE Alaska, C mobilization rates are likely higher than determined in this study.

The period of time for carbon to recover after a landslide disturbance is difficult to ascertain, due to a lack of research in this area, so determining the magnitude of the landslide carbon source or sink effect at different time scales remains an open question. Previous studies in SE Alaska found aboveground carbon (C_{bio}) initially accumulating at 300 tC km^{-2} yr^{-1} in logged forests, reaching a steady state density of 25,000 tC km^{-2} in unmanaged forests older than 350 years (Leighty et al., 2006). C_{bio} accretion rates on landslides are likely slower due to the evacuation of soils, which require a period of time to re-develop and thus delay ecologic succession post-disturbance (Reneau & Dietrich, 1991; Reneau et al., 1990). Infilling of sediment on the margins of a debris flow track would likely expedite C recovery on a landslide scar. Additionally, there are differences between secondary (some biomass still remains after disturbance) and primary (biomass completely gone) ecologic succession (Kimmins, 2004). Using the 300 tC km^{-2} yr^{-1} C_{bio} recovery for logged forests, it would take 110 years for mobilized C_{bio} to recover from the 2015 event, which is likely a minimum because it does not account for the delay in ecologic succession as a result of soil evacuation by landslides. On the other hand, SOC requires longer periods of time (on the order of millenniums) to recover relative to C_{bio} on the disturbed slopes due to the slow processes which accumulate organic material in soils (Kramer

et al., 2004). Windthrow disturbances in SE Alaskan watersheds were found to be drivers of SOC respiration by exhuming soil (Kramer et al., 2004). For landslide disturbances, organic soil stripped from slopes can be exposed at the surface in the deposit, where it can decompose and respire C to the atmosphere, but a greater portion of the mobilized soil is buried in the deposit relative to windthrow disturbances, resulting in short-term sequestration. Hillslope deposits can result in a net carbon sink or source depending on the rates of decomposition of mobilized C_{bio} and SOC, and the recovery of total C on the disturbed slope, but further research within the study area is required to make this distinction.

For the remaining 61% of stream deposited material, we take into consideration Holocene carbon burial rates within fjords, and total organic carbon in continental shelf sediment in the study region to assess the potential for those deposits to sequester C. In the context of our TNF landsliding rate of 2.46 ± 0.12 tC km^{-2} yr^{-1}, only 10% of the mobilized C would need to be exported to fjords to sustain the measured burial rate of 0.265 tC km^{-2} yr^{-1} (Cui et al., 2016; Smith et al., 2015). This amount is nearly sustained through the amount of carbon deposited to large order streams, with our rate of 0.22 ± tC km^{-1} yr^{-1} of carbon deposited into mainstem streams. With that in mind, not all of the mainstem streams terminate at fjords, and instead many leads directly to the ocean. Future work on secondary transport mechanisms within smaller streams would help understand the export efficiency of carbon from these systems. It is reasonable to conclude that C mobilizing landslide events are contributing to the globally high rate of C burial in SE Alaskan fjords, but the precise proportion of POC transported from landslide deposits in streams to fjords is unknown. So, although C mobilization amount and rates in SE Alaska are generally low compared to areas with more extreme disturbances, the high connectivity of landslide deposits to the ocean and fjords via small mountain streams likely facilitates a high rate of carbon sequestration over geologic timescales, with valley configuration playing a role in how the material is exported. This is consistent with observations of earthquake-triggered landslides in southeast Asia, where high connectivity to streams make landslides net sink in the years following an earthquake event, as a result of efficient export of sediment to the ocean (Croissant et al., 2020). However, some C in the form of dissolved organic carbon (DOC) can be lost to the atmosphere as it transports. It is likely that landslide disturbances, which transport rather than remove C from the landscape, contribute to the high stream DOC levels in SE Alaska, with an average of 18,700 ± 1,090 tC yr^{-1} being deposited into streams in the entire TNF. Despite some C being lost due to the atmosphere, landslides probably still contribute to the high accumulation rates in fjords.

Directly depositing material into fjord waters could also be a potential source for the higher C accumulation rates in SE Alaskan fjords (Cui et al., 2016; Smith et al., 2015). While few of the debris flows simulated with DFLOWZ deposited directly into fjords or to the open Pacific Ocean due to a smaller area of interest being analyzed, field observations and mapped landslides indicated deposition frequently occurring directly into bodies of water. Based on aerial imagery of landslides initiated during the 2015 storm, 27% of the deposits occurred directly into or adjacent to a body of water. The rate at which this occurs is likely higher in SE Alaska relative to other debris flow susceptible landscapes due to steep slopes adjacent to fjords and the Pacific Ocean. The 2015 storm in particular primarily initiated landslides along the outer coast, causing more direct deposition into the Pacific Ocean, rather than deposition into fjords, which is the case for many landslides occurring throughout southeast Alaska. In regards to ocean-delivered POC, continental shelves provide an opportunity for long-term storage of mobilized C if it becomes buried. Sedimentation from fresh water discharge flowing from watersheds allows for transported POC to be buried in deltas on the SE Alaskan continental shelf, which is supported by the identification of land-derived C (1%–8% by weight) contained within coastal sediments (Walinsky et al., 2009). Landsliding allows additional sedimentation to occur on the coast, thus increasing the chance of POC to become buried if delivered to the continental shelf. Further research on the portion of CWD breaking down into POC and how much becomes buried in marine sediments would further constrain the magnitude of this geologic carbon sink.

4.2. Simulated Debris Flow Deposition and Carbon Mobilization "Hotspots"

We utilized a long-term debris flow inundation model to analyze stream connectivity for mobilized carbon, but this method could be improved in the future by incorporating landscape evolution as debris flows occur across the study area. Using a DEM collected over a small period of time that represents elevations as an input to a long-term model could result in an over-estimation of the number of times a location is

inundated, and an under-estimation of the spatial extent of inundation, since each debris flow is simulated independently on the same topography. Future work could therefore involve a debris flow inundation model in combination with a landscape evolution model to refine the spatial distribution of deposited C. However, our approach produced similar stream connectivity of deposits to the 2015 debris flows, indicating it is a reasonable first order approach. The modeled connectivity rate is higher than that of the 1960–2015 TNF Landslide Inventory is likely the result of using the D-8 flow direction algorithm for both the modeled stream network and the debris flow runout paths. By definition, the modeled deposits followed the same routes used to define the streams, so they were not connected only when debris flow runout was less than the drainage area threshold.

Our modeling results for debris flow deposition across the landscape of northern Baranof Island provide a unique opportunity to observe depositional "hotspots" for mobilized carbon that likely represent Holocene-scale patterns. Additionally, these depositional hotspots represent localized carbon sinks from the atmosphere, which together cause SE Alaska to be a major region for carbon sequestration. Slopes or streams that are immediately downslope from steep topography typically are inundated by deposition multiple times since multiple flow paths from different initiation sites tend to converge in such areas. The depositional start for the simulations at a slope threshold of 20° coincides with our field observations and previously measured landslide depositional slopes in the region (Booth et al., 2020; Johnson et al., 2000). It should be noted, however, that the initiation of landslide deposition is not solely dependent on a single slope threshold, but can be influenced by factors such as forest density and flow behavior (Fannin & Wise, 2001). Debris flows that recur at the same site before vegetation has had time to recover may therefore have different runout characteristics than debris flows occurring in undisturbed forests, which is an assumption in our runout simulations.

Our study directly considered the relationship between landslide disturbances and C stocks within the TNF and showed that moderate landslide disturbance in areas with dense C stocks resulted in the highest C mobilization rates. This differs from other forest disturbance events such as fires or insect infestations, which have the capacity to scale with available carbon. The result that C mobilization density is higher in regions that have higher C stocks coupled with moderate landslide density (Figure 5) supports the ecological theory that higher C stocks correlate with moderate disturbances (Buma & Thompson, 2019; McLauchlan et al., 2014). This is due to high disturbance regimes having very frequent events which do not provide an opportunity for carbon to be re-established over the landscape, while low disturbance regimes experience biogeochemical limitations with the lack of nutrient recycling (Peltzer, et al., 2010). As carbon is transported from high on hillslopes to downslope sites where it is either buried or transported down streams, ecologic succession occurs on the disturbed slopes, contributing as a long-term carbon accreting mechanism. This process compounds over time as landslide-triggering storms allow for moderately disturbed areas to sequester large amounts of carbon at millennial timescales.

4.3. Implications for Future Carbon Mobilization

Projected changes for SE Alaskan climate predict precipitation increase by 6%–18% in the next century (Shanley et al., 2015). The atmospheric rivers that bring strong storms to SE Alaska have been observed as occurring more frequently in the past century (Sharma & Déry, 2020). This increase in annual precipitation is likely to trigger additional landslides by making high-intensity and duration rain storms more frequent (Crozier, 2010). A direct result of increased landslide rates is additional C mobilization, and the short to long-term sequestration in soils and marine settings, providing a buffer to increasing atmospheric CO_2 levels, albeit minor compared to ongoing global-scale anthropogenic CO_2 emissions.

Previous research for implications of climate change in SE Alaska primarily focuses on changes in net primary productivity (NPP), volumetric loss of glaciers, and impacts on fish habitats (Haufler, 2010; Shanley et al., 2015). A projected 20% increase in NPP for spruces is estimated for Alaska due to warming temperatures, but with this shift in climate comes an increase in respiration and decomposition processes (Keyser et al., 2000). With this projected increase in mind, a similar increase in landslide rates would be required to maintain the carbon accreting mechanism we have identified in this study.

5. Conclusions

We utilized landslide mapping and runout modeling in SE Alaska in conjunction with geospatial carbon density models of SOC and C_{bio} to estimate the amount of carbon mobilized by debris flows in SE Alaskan forests at two different spatio-temporal scales and predicted runout locations for 10-ky timescales. A single storm in August 2015 mobilized 57,651 ± 3,266 tC, while debris flows across the entire TNF (70,5876 km^2) mobilized 4.69 ± 0.21 MtC, a rate of 2.46 ± 0.12 tC km^{-2} yr^{-1} over the 55-year period analyzed. The annual rate is lower relative to other large-scale, landslide-mobilizing carbon events recorded in the world, such as tropical storms that impact SE Asia (~7 tC km^{-2} yr^{-1}) or earthquake-triggered landslide events (~9 tC km^{-2} yr^{-1}), primarily due to the higher rate of landslide area triggered by those events. However, the geomorphic setting where landslides deposit can influence the depositional fate of mobilized carbon, affecting the temporal scale for C sequestration from the atmospheric pool. About 71.2% of the landslides that occurred during the 2015 storm event (78.9% for our long-term inundation modeled deposits) were connected to the stream network, while 60.1% of landslides from our analysis on the entire TNF landslide inventory were connected. So, although the rate of C mobilization by debris flows in SE Alaska may be relatively low, much of that C may be efficiently transferred to marine basins, where it can become sequestered over geologic time scales, implying that SE Alaska is an ideal location for carbon sequestration. Furthermore, we found that C mobilization typically corresponds to moderate landslide frequency coupled with high C density, a result that may indicate SE Alaskan landslides contribute to the globally high carbon density of its forests. The depositional fate of stream and hillslope delivered C indicates that landslides impact the regional carbon budget cycle, by mobilizing carbon at a rate close to the net loss amount caused by logging within the region. This work supports the emerging view that the link between landslide forest disturbances and erosion of organic carbon plays an important role in the global carbon cycle over geologic timescales.

Conflict of Interest

The authors declare no conflicts of interests relevant to this study.

Data Availability Statement

Tongass Landslide Inventory for mobilization estimates are publically available at: Tongass National Forest (2019). VAB data set for calibrating debris flow runout modeling is available at: Booth et al. (2020). Software for debris flow runout simulations are available at: Berti (2014). Carbon models for mobilization estimations is available at: Buma and Thompson (2019). Landslide initiation susceptibility data used for debris flow runout simulations are available at: Buma and Johnson (2015).The 5m DEM used for landslide modeling is available at U.S. Geological Survey (2017). Landslide planimetric area and estimated carbon mobilization amounts used in the study is available at Vascik (2021a). Debris flow inundation model results used in the study is available at Vascik (2021b).

Acknowledgments
This project received funding from NSF Award EAR-1711986 to Booth. The authors would like to thank the following field assistants for their contributions: C. Seibert, C. Sifford, D. de Guzman, K. Turchick, and the Sitka Sound Science Center for their hospitality.

References

Aller, R. C. (1998). Mobile deltaic and continental shelf muds as suboxic, fluidized bed reactors. *Marine Chemistry*, *61*(3–4), 143–155. https://doi.org/10.1016/s0304-4203(98)00024-3

Barrett, T. M., & Christensen, G. A. (2011). *Forests of southeast and south-central Alaska, 2004–2008: Five-year forest inventory and analysis report. Gen. Tech. Rep. PNW-GTR-835* (Vol. 156, p. 835). US Department of Agriculture, Forest Service.

Barth, S., Geertsema, M., Bevington, A. R., Bird, A. L., Clague, J. J., Millard, T., et al. (2020). Landslide response to the 27 October 2012 earthquake (MW 7.8), southern Haida Gwaii, British Columbia, Canada. *Landslides*, *17*(3), 517–526. https://doi.org/10.1007/s10346-019-01292-7

Benda, L. E., & Cundy, T. W. (1990). Predicting deposition of debris flows in mountain channels. *Canadian Geotechnical Journal*, *27*(4), 409–417. https://doi.org/10.1139/t90-057

Berg, E. C., Gale, C. B., Morgan, T. A., Brackley, A. M., Keegan, C. E., Alexander, S. J., et al. (2014). *Alaska's timber harvest and forest products industry, 2011. Gen. Tech. Rep. PNW GTR-903* (Vol. 39, p. 903). US Department of Agriculture, Forest Service.

Berhe, A. A., Harte, J., Harden, J. W., & Torn, M. S. (2007). The significance of the erosion-induced terrestrial carbon sink. *BioScience*, *57*(4), 337–346. https://doi.org/10.1641/b570408

Berti, M. (2014). *"DFLOWZ"*. Università di Bologna—Italy. Retrieved from http://137.204.103.162/dflowz/dflowz.htm

Berti, M., & Simoni, A. (2007). Prediction of debris flow inundation areas using empirical mobility relationships. *Geomorphology*, *90*(1–2), 144–161. https://doi.org/10.1016/j.geomorph.2007.01.014

Booth, A. M., Sifford, C., Vascik, B., Siebert, C., & Buma, B. (2020). Large wood inhibits debris flow runout in forested southeast Alaska. *Earth Surface Processes and Landforms*, *45*, 1555–1568. https://doi.org/10.1002/esp.4830

Buma, B., & Johnson, A. C. (2015). The role of windstorm exposure and yellow cedar decline on landslide susceptibility in southeast Alaskan temperate rainforests. *Geomorphology*, *228*, 504–511. https://doi.org/10.1016/j.geomorph.2014.10.014

Buma, B., & Thompson, T. (2019). Long-term exposure to more frequent disturbances increases baseline carbon in some ecosystems: Mapping and quantifying the disturbance frequency-ecosystem C relationship. *PLoS One*, *14*(2), e0212526. https://doi.org/10.1371/journal.pone.0212526

Burdige, D. J. (2005). Burial of terrestrial organic matter in marine sediments: A re-assessment. *Global Biogeochemical Cycles*, *19*(4). https://doi.org/10.1029/2004gb002368

Chambers, J. Q., Schimel, J. P., & Nobre, A. D. (2001). Respiration from coarse wood litter in central Amazon forests. *Biogeochemistry*, *52*(2), 115–131. https://doi.org/10.1023/a:1006473530673

Clark, K. E., West, A. J., Hilton, R. G., Asner, G. P., Quesada, C. A., Silman, M., et al. (2016). Storm-triggered landslides in the Peruvian Andes and implications for topography, carbon cycles, and biodiversity. *Earth Surface Dynamics*, *4*(1), 47–70. https://doi.org/10.5194/esurf-4-47-2016

Croissant, T., Hilton, R. G., Li, G., Howarth, J., Wang, J., Harvey, E. L., et al. (2020). Pulsed carbon export from mountains by earthquake-triggered landslides explored in a reduced-complexity model. *Earth Surface Dynamics Discussions*, 1–39.

Crosta, G. B., Cucchiaro, S., & Frattini, P. (2003). Validation of semi-empirical relationships for the definition of debris-flow behavior in granular materials. *Presented at the Proceedings of the third International Conference on debris-flow hazards Mitigation: Mechanics, prediction and assessment* (pp. 821–831). MillPress, Rotterdam.

Crozier, M. J. (2010). Deciphering the effect of climate change on landslide activity: A review. *Geomorphology*, *124*(3–4), 260–267. https://doi.org/10.1016/j.geomorph.2010.04.009

Cui, P., Hu, K., Zhuang, J., Yang, Y., & Zhang, J. (2011). Prediction of debris-flow danger area by combining hydrological and inundation simulation methods. *Journal of Mountain Science*, *8*(1), 1–9. https://doi.org/10.1007/s11629-011-2040-8

Cui, X., Bianchi, T. S., Savage, C., & Smith, R. W. (2016). Organic carbon burial in Fjords: Terrestrial versus marine inputs. *Earth and Planetary Science Letters*, *451*, 41–50. https://doi.org/10.1016/j.epsl.2016.07.003

Currie, W. S., Yanai, R. D., Piatek, K. B., Prescott, C. E., & Goodale, C. L. (2002). Processes affecting carbon storage in the forest floor and in downed woody debris. In *The Potential of US Forest Soils to Sequester Carbon and Mitigate the Greenhouse Effect*, 135–157. https://doi.org/10.1201/9781420032277-9

Doser, D. I., Pelton, J. R., & Veilleux, A. M. (1997). Earthquakes in the Pamplona zone, Yakutat block, south central Alaska. *Journal of Geophysical Research: Solid Earth*, *102*(B11), 24499–24511. https://doi.org/10.1029/97jb01729

Eaton, L. S., Benjamin A., M., Craig Kochel, R., & Howard, A. D. (2003). Role of debris flows in long-term landscape denudation in the Central Appalachians of Virginia. *Geology*, *31*(4), 339–342. https://doi.org/10.1130/0091-7613(2003)031<0339:rodfil>2.0.co;2

Falkowski, P., Scholes, R. J., Boyle, E., Canadell, J., Canfield, D., Elser, J., et al. (2000). The global carbon cycle: A test of our knowledge of earth as a system. *Science*, *290*(5490), 291–296. https://doi.org/10.1126/science.290.5490.291

Fannin, R. J., & Wise, M. P. (2001). An empirical-statistical model for debris flow travel distance. *Canadian Geotechnical Journal*, *38*(5), 982–994. https://doi.org/10.1139/t01-030

Frith, N. V., Hilton, R. G., Howarth, J. D., Gröcke, D. R., Fitzsimons, S. J., Croissant, T., et al. (2018). Carbon export from mountain forests enhanced by earthquake-triggered landslides over millennia. *Nature Geoscience*, *11*(10), 772–776. https://doi.org/10.1038/s41561-018-0216-3

Galy, V., France-Lanord, C., Beyssac, O., Faure, P., Kudrass, H., & Palhol, F. (2007). Efficient organic carbon burial in the Bengal Fan sustained by the Himalayan erosional system. *Nature*, *450*(7168), 407–410. https://doi.org/10.1038/nature06273

Gehrels, G., Berg, H., & Plafker, G. (1994). *Geology of southeastern Alaska*. The Geology of Alaska.

Gomi, T., Sidle, R. C., & Swanston, D. N. (2004). Hydrogeomorphic linkages of sediment transport in headwater streams, Maybeso experimental forest, Southeast Alaska. *Hydrological Processes*, *18*(4), 667–683. https://doi.org/10.1002/hyp.1366

Goñi, M. A., Hatten, J. A., Wheatcroft, R. A., & Borgeld, J. C. (2013). Particulate organic matter export by two contrasting small mountainous rivers from the Pacific Northwest, USA. *Journal of Geophysical Research: Biogeosciences*, *118*(1), 112–134.

Gough, C. M., Vogel, C. S., Clare, K., Nagel, L., Flower, C. E., & Curtis, P. S. (2007). Coarse woody debris and the carbon balance of a North Temperate Forest. *Forest Ecology and Management*, *244*(1–3), 60–67. https://doi.org/10.1016/j.foreco.2007.03.039

Guthrie, R. H., Hockin, A., Colquhoun, L., Nagy, T., Evans, S. G., & Ayles, C. (2010). An examination of controls on debris flow mobility: Evidence from coastal British Columbia. *Geomorphology*, *114*(4), 601–613. https://doi.org/10.1016/j.geomorph.2009.09.021

Guzzetti, F., Peruccacci, S., Rossi, M., Colin, P., & Stark (2008). The rainfall intensity–duration control of shallow landslides and debris flows: An update. *Landslides*, *5*(1), 3–17. https://doi.org/10.1007/s10346-007-0112-1

Hafner, S. D., Groffman, P. M., & Mitchell, M. J. (2005). Leaching of dissolved organic carbon, dissolved organic nitrogen, and other solutes from coarse woody debris and litter in a mixed forest in New York State. *Biogeochemistry*, *74*(2), 257–282. https://doi.org/10.1007/s10533-004-4722-6

Hamilton, T., & Thorson, R. (1983). The Cordilleran ice sheet in Alaska. In The late Pleistocene. Late Quaternary Environments of the United States (Vol. 1). University of Minnesota Press.

Hamilton, T. D. (1994). Late Cenozoic glaciation of Alaska. *The Geology of Alaska*, *1*, 813–844.

Harris, A. S. (1989). *Wind in the forests of southeast Alaska and Guides for reducing damage* (Vol. 244). US Department of Agriculture, Forest Service, Pacific Northwest Research Station.

Haufler, J. (2010). *Climate change: Anticipated effects on ecosystem services and potential actions by the Alaska Region*. US Forest Service. DIANE Publishing.

Hilton, R. G., Meunier, P., Hovius, N., Bellingham, P. J., & Galy, A. (2011). Landslide impact on organic carbon cycling in a temperate montane forest. *Earth Surface Processes and Landforms*, *36*(12), 1670–1679. https://doi.org/10.1002/esp.2191

Hilton, R. G., & West, A. J. (2020). Mountains, erosion and the carbon cycle. *Nature Reviews Earth & Environment*, *1*(6), 284–299. https://doi.org/10.1038/s43017-020-0058-6

Horel, J., Splitt, M., Dunn, L., Pechmann, J., White, B., Ciliberti, C., et al. (2002). Mesowest: Cooperative mesonets in the western United States. *Bulletin of the American Meteorological Society*, *83*(2), 211–225. https://doi.org/10.1175/1520-0477(2002)083<0211:mcmitw>2.3.co;2

Houghton, J., Meira Filho, L., Lim, K., Trennton, I., Mamaty, I., Bonduki, Y., et al. (1997). Revised 1996 IPCC Guidelines for National Greenhouse Gas inventories. In Intergovernmental Panel on Climate Change (Vol. 1–3). Cambridge University Press.

Hovius, N., Stark, C. P., & Allen, P. A. (1997). Sediment flux from a mountain belt derived by landslide mapping. *Geology*, *25*(3), 231–234. https://doi.org/10.1130/0091-7613(1997)025<0231:sffamb>2.3.co;2

Iverson, R. M. (1997). The physics of debris flows. *Reviews of Geophysics*, *35*(3), 245–296. https://doi.org/10.1029/97RG00426

Iverson, R. M., Reid, M. E., & LaHusen, R. G. (1997). Debris-flow mobilization from landslides. *Annual Review of Earth and Planetary Sciences*, *25*(1), 85–138. https://doi.org/10.1146/annurev.earth.25.1.85

Iverson, R. M., Schilling, S. P., & Vallance, J. W. (1998). Objective delineation of lahar-inundation hazard zones. *The Geological Society of America Bulletin*, *110*(8), 972–984. https://doi.org/10.1130/0016-7606(1998)110<0972:odolih>2.3.co;2

Jensen, D. W., Ashley Steel, E., Fullerton, A. H., & Pess, G. R. (2009). Impact of fine sediment on egg-to-fry survival of Pacific Salmon: A meta-analysis of published studies. *Reviews in Fisheries Science*, *17*(3), 348–359. https://doi.org/10.1080/10641260902716954

Johnson, A. C., Swanston, D. N., & McGee, K. E. (2000). Landslide initiation, runout, and deposition within clearcuts and old-growth forests of Alaska. *JAWRA Journal of the American Water Resources Association*, *36*(1), 17–30. https://doi.org/10.1111/j.1752-1688.2000.tb04245.x

Kaufman, D. S., & Manley, W. F. (2004). Pleistocene maximum and Late Wisconsinan glacier extents across Alaska, USA. In Developments in Quaternary Sciences (Vol. 2, pp. 9–27). Elsevier. https://doi.org/10.1016/s1571-0866(04)80182-9

Keith, H., Mackey, B. G., & Lindenmayer, D. B. (2009). Re-evaluation of forest biomass carbon stocks and lessons from the world's most carbon-dense forests. *Proceedings of the National Academy of Sciences*, *106*(28), 11635–11640. https://doi.org/10.1073/pnas.0901970106

Keyser, A. R., Kimball, J. S., Nemani, R. R., & Running, S. W. (2000). Simulating the effects of climate change on the carbon balance of North American high-latitude forests. *Global Change Biology*, *6*(S1), 185–195. https://doi.org/10.1046/j.1365-2486.2000.06020.x

Kimmins, J. P. (2004). Forest ecology. *Fishes and Forestry: Worldwide Watershed Interactions and Management*, *17–43*.

Korup, O., & Rixen, C. (2014). Soil erosion and organic carbon export by wet snow avalanches. *The Cryosphere*, *8*(2), 651–658. https://doi.org/10.5194/tc-8-651-2014

Kramer, M. G., Hansen, A. J., Taper, M. L., & Kissinger, E. J. (2001). Abiotic controls on long-term windthrow disturbance and temperate rain forest dynamics in Southeast Alaska. *Ecology*, *82*(10), 2749–2768. https://doi.org/10.1890/0012-9658(2001)082[2749:acoltw]2.0.co;2

Kramer, M. G., Sollins, P., & Sletten, R. S. (2004). Soil carbon dynamics across a windthrow disturbance sequence in southeast Alaska. *Ecology*, *85*(8), 2230–2244. https://doi.org/10.1890/02-4098

Lancaster, S. T., Hayes, S. K., & Grant, G. E. (2003). Effects of wood on debris flow runout in small mountain watersheds: Effects of wood on debris flow runout. *Water Resources Research*, *39*(6). https://doi.org/10.1029/2001WR001227

Leighty, W. W., Hamburg, S. P., & Caouette, J. (2006). Effects of management on carbon sequestration in forest biomass in Southeast Alaska. *Ecosystems*, *9*(7), 1051–1065. https://doi.org/10.1007/s10021-005-0028-3

Li, G., West, A. J., Densmore, A. L., Hammond, D. E., Jin, Z., Zhang, F., et al. (2016). Connectivity of earthquake-triggered landslides with the fluvial network: Implications for landslide sediment transport after the 2008 Wenchuan earthquake. *Journal of Geophysical Research: Earth Surface*, *121*(4), 703–724. https://doi.org/10.1002/2015jf003718

Li, G., West, A. J., Densmore, A. L., Jin, Z., Parker, R. N., & Hilton, R. G. (2014). Seismic mountain building: Landslides associated with the 2008 Wenchuan earthquake in the context of a generalized model for earthquake volume balance. *Geochemistry, Geophysics, Geosystems*, *15*(4), 833–844. https://doi.org/10.1002/2013gc005067

Madej, M. A. (2010). Redwoods, restoration, and implications for carbon budgets. *Geomorphology*, *116*(3–4), 264–273. https://doi.org/10.1016/j.geomorph.2009.11.012

Marra, J. L., & Edmonds, R. L. (1994). Coarse woody debris and forest floor respiration in an old-growth coniferous forest on the Olympic Peninsula, Washington, USA. *Canadian Journal of Forest Research*, *24*(9), 1811–1817. https://doi.org/10.1139/x94-234

May, C. L. (2002). Debris flows through different forest age classes in the Central Oregon Coast Range. *JAWRA Journal of the American Water Resources Association*, *38*(4), 1097–1113. https://doi.org/10.1111/j.1752-1688.2002.tb05549.x

McLauchlan, K. K., Higuera, P. E., Gavin, D. G., Perakis, S. S., Mack, M. C., Alexander, H., et al. (2014). Reconstructing disturbances and their biogeochemical consequences over multiple timescales. *BioScience*, *64*(2), 105–116. https://doi.org/10.1093/biosci/bit017

McNicol, G., Bulmer, C., D'Amore, D., Sanborn, P., Saunders, S., Giesbrecht, I., et al. (2019). Large, climate-sensitive soil carbon stocks mapped with pedology-informed machine learning in the North Pacific coastal temperate rainforest. *Environmental Research Letters*, *14*(1), 014004. https://doi.org/10.1088/1748-9326/aaed52

Melillo, J. M., David McGuire, A., Kicklighter, D. W., Moore, B., III, Vorosmarty, C. J., & Schloss, A. L. (1993). Global climate change and terrestrial net primary production. *Nature; London*, *363*(6426), 234–240. https://doi.org/10.1038/363234a0

Mohr, C. H., Korup, O., Ulloa, H., & Iroumé, A. (2017). Pyroclastic eruption boosts organic carbon fluxes into Patagonian fjords. *Global Biogeochemical Cycles*, *31*(11), 1626–1638. https://doi.org/10.1002/2017gb005647

Neal, C. A., McGimsey, R. G., Gardner, C. A., Harbin, M. L., & Nye, C. J. (1995). Tephra-fall deposits from the 1992 eruptions of Crater Peak, Mount Spurr Volcano, Alaska: A preliminary report on distribution, stratigraphy, and composition. *US Geological Survey Bulletin*, *2139*, 65–79.

O'Callaghan, J. F., & Mark, D. M. (1984). The extraction of drainage networks from digital elevation data. *Computer Vision, Graphics, and Image Processing*, *28*(3), 323–344.

Peltzer, D. A., Wardle, D. A., Allison, V. J., Baisden, W. T., Bardgett, R. D., Chadwick, O. A., et al. (2010). Understanding ecosystem retrogression. *Ecological Monographs*, *80*(4), 509–529. https://doi.org/10.1890/09-1552.1

Progar, R., Schowalter, T., Freitag, C., & Morrell, J. J. (2000). Respiration from coarse woody debris as affected by moisture and saprotroph functional diversity in Western Oregon. *Oecologia*, *124*(3), 426–431. https://doi.org/10.1007/pl00008868

Raich, J. W., & Schlesinger, W. H. (1992). The global carbon dioxide flux in soil respiration and its relationship to vegetation and climate. *Tellus B: Chemical and Physical Meteorology*, *44*(2), 81–99. https://doi.org/10.1034/j.1600-0889.1992.t01-1-00001.x

Ramos Scharrón, C. E., Castellanos, E. J., & Restrepo, C. (2012). The transfer of modern organic carbon by landslide activity in tropical montane ecosystems. *Journal of Geophysical Research: Biogeosciences*, *117*(G3). https://doi.org/10.1029/2011JG001838

Reid, M. E., Coe, J. A., & Brien, D. L. (2016). Forecasting inundation from debris flows that grow volumetrically during travel, with application to the Oregon Coast Range, USA. *Geomorphology*, *273*, 396–411. https://doi.org/10.1016/j.geomorph.2016.07.039

Reneau, S. L., & Dietrich, W. E. (1991). Erosion rates in the southern Oregon Coast Range: Evidence for an equilibrium between hillslope erosion and sediment yield. *Earth Surface Processes and Landforms*, *16*(4), 307–322. https://doi.org/10.1002/esp.3290160405

Reneau, S. L., Dietrich, W. E., Donahue, D. J., Jull, A. T., & Rubin, M. (1990). Late Quaternary history of colluvial deposition and erosion in hollows, central California Coast Ranges. *The Geological Society of America Bulletin*, *102*(7), 969–982. https://doi.org/10.1130/0016-7606(1990)102<0969:lqhocd>2.3.co;2

Restrepo, C., Walker, L. R. A. B. S., Shiels, A. B., Bussmann, R., Claessens, L., Fisch, S., et al. (2009). Rainer Bussmann, Lieven Claessens, Simey Fisch, Pablo Lozano, Girish Negi, Leonardo Paolini, Germán Poveda, and others landsliding and its multiscale influence on mountainscapes. *BioScience*, *59*(8), 685–698. https://doi.org/10.1525/bio.2009.59.8.10

Rickenmann, D. (1999). Empirical relationships for debris flows. *Natural Hazards*, *19*(1), 47–77. https://doi.org/10.1023/a:1008064220727

Riehle, J. R., Champion, D. E., Brew, D. A., & Lanphere, M. A. (1992). Pyroclastic deposits of the Mount Edgecumbe volcanic field, southeast Alaska: Eruptions of a stratified magma chamber. *Journal of Volcanology and Geothermal Research*, *53*(1–4), 117–143. https://doi.org/10.1016/0377-0273(92)90078-r

Rumpel, C., Kögel-Knabner, I., & Bruhn, F. (2002). Vertical distribution, age, and chemical composition of organic carbon in two forest soils of different pedogenesis. *Organic Geochemistry*, *33*(10), 1131–1142. https://doi.org/10.1016/s0146-6380(02)00088-8

Russell, M. B., Fraver, S., Aakala, T., Gove, J. H., Woodall, C. W., D'Amato, A. W., & Ducey, M. J. (2015). Quantifying carbon stores and decomposition in dead wood: A review. *Forest Ecology and Management*, *350*, 107–128. https://doi.org/10.1016/j.foreco.2015.04.033

Scheidl, C., & Rickenmann, D. (2010). Empirical prediction of debris-flow mobility and deposition on fans. *Earth Surface Processes and Landforms*, *35*(2), 157–n. https://doi.org/10.1002/esp.1897

Schilling, S. P. (1998). *LAHARZ; GIS programs for automated mapping of lahar-inundation hazard zones*. US Geological Survey; Information Services.

Schimel, D. S., Braswell, B., Holland, E. A., McKeown, R., Ojima, D. S., Painter, T. H., et al. (1994). Climatic, edaphic, and biotic controls over storage and turnover of carbon in soils. *Global Biogeochemical Cycles*, *8*(3), 279–293. https://doi.org/10.1029/94gb00993

Schroeder, W. L. (1983). *Geotechnical properties of southeast Alaskan forest soils* (pp. 1–46). Oregon State University.

Segoni, S., Piciullo, L., & Gariano, S. L. (2018). A Review of the recent literature on rainfall thresholds for landslide occurrence. *Landslides*, *15*(8), 1483–1501. https://doi.org/10.1007/s10346-018-0966-4

Shanley, C. S., Pyare, S., Goldstein, M. I., Alaback, P. B., Albert, D. M., Beier, C. M., et al. (2015). Climate change implications in the northern coastal temperate rainforest of North America. *Climatic Change*, *130*(2), 155–170. https://doi.org/10.1007/s10584-015-1355-9

Sharma, A. R., & Déry, S. J. (2020). Variability and trends of landfalling atmospheric rivers along the Pacific Coast of Northwestern North America. *International Journal of Climatology*, *40*(1), 544–558. https://doi.org/10.1002/joc.6227

Shulski, M., & Wendler, G. (2007). *The climate of Alaska*. University of Alaska Press.

Sidle, R. C. (1988). Bed load transport regime of a small forest stream. *Water Resources Research*, *24*(2), 207–218. https://doi.org/10.1029/wr024i002p00207

Silverman, B. W. (1986). *Density estimation for statistics and data analysis* (Vol. 26). CRC press.

Sitka Geotask Force. (2016). *Summaries August 2015 Sitka landslides*. Sitka Sound Science Center.

Smith, R. W., Bianchi, T. S., Allison, M., Savage, C., & Galy, V. (2015). High rates of organic carbon burial in fjord sediments globally. *Nature Geoscience*, *8*(6), 450–453. https://doi.org/10.1038/ngeo2421

SNAP. (2018). *Scenarios network for Alaska and Arctic planning: Historical monthly temperature and precipitation and historical derived temperature products*.

Stallard, R. F. (1998). Terrestrial sedimentation and the carbon cycle: Coupling weathering and erosion to carbon burial. *Global Biogeochemical Cycles*, *12*(2), 231–257. https://doi.org/10.1029/98GB00741

Stock, J. D., & Dietrich, W. E. (2006). Erosion of steepland valleys by debris flows. The *Geological Society of America Bulletin*, *118*(9–10), 1125–1148. https://doi.org/10.1130/b25902.1

Strahler, A. N. (1957). Quantitative analysis of watershed geomorphology. *Eos, Transactions American Geophysical Union*, *38*(6), 913–920. https://doi.org/10.1029/tr038i006p00913

Tarboton, D. G., Bras, R. L., & Rodriguez-Iturbe, I. (1991). On the extraction of channel networks from digital elevation data. *Hydrological Processes*, *5*(1), 81–100. https://doi.org/10.1002/hyp.3360050107

Tongass National Forest. (2019), *USDA forest Service R10*. Tongass National Forest. Retrieved from https://hub.arcgis.com/datasets/e2f7e4b47b434f1c873ac3278717f801_0

Triska, F. J., & Cromack, K., Jr. (1980). The role of wood debris in forests and streams. In *Forests: Fresh Perspectives from ecosystem Analysis* (pp. 171–190). Oregon State University Press.

U.S. Geological Survey. (2017). *5 meter Alaska digital elevation models (DEMs)—USGS National map 3DEP. Downloadable data collection*. U.S. Geological Survey.

U.S. Geological Survey. (2018). National Geospatial Program. In *USGS National Hydrography dataset (NHD) best resolution HU8-9 20180304 for HU-8 Subbasin FileGDB 10.1 model*.

Varnes, D. J. (1958). Landslide types and processes. *Landslides and Engineering Practice*, *24*, 20–47.

Vascik, B. (2021a). *Debris flow carbon mobilization table ver 1. Environmental data initiative*. https://doi.org/10.6073/pasta/fbdd78ffb9913ec1557406c6569ad8be

Vascik, B. (2021b). *Sitka debris flow inundation model ver 1. Environmental data initiative*. https://doi.org/10.6073/pasta/744fc1753cdcb301755f904298c1927f

Walinsky, S., Prahl, F., Mix, A., Finney, B., Jaeger, J., & Rosen, G. (2009). Distribution and composition of organic matter in surface sediments of coastal Southeast Alaska. *Continental Shelf Research*, *29*(13), 1565–1579. https://doi.org/10.1016/j.csr.2009.04.006

Wang, J., Jin, Z., Hilton, R. G., Zhang, F., Li, G., Densmore, A. L., et al. (2016). Earthquake-triggered increase in biospheric carbon export from a mountain belt. *Geology*, *44*(6), 471–474. https://doi.org/10.1130/g37533.1

Wang, Y., Law, R., & Pak, B. (2010). A global model of carbon, nitrogen and phosphorus cycles for the terrestrial biosphere. *Biogeosciences*, *7*(7), 2261–2282. https://doi.org/10.5194/bg-7-2261-2010

Wendler, G., Galloway, K., & Stuefer, M. (2016). On the climate and climate change of Sitka, Southeast Alaska. *Theoretical and Applied Climatology*, *126*(1–2), 27–34. https://doi.org/10.1007/s00704-015-1542-7

West, A. J., Lin, C.-W., Lin, T.-C., Hilton, R. G., Liu, S.-H., Chang, C.-T., et al. (2011). Mobilization and transport of coarse woody debris to the oceans triggered by an extreme tropical storm. *Limnology & Oceanography*, *56*(1), 77–85. https://doi.org/10.4319/lo.2011.56.1.0077

Wiebe, S. A., Morris, D. M., Luckai, N. J., & Reid, D. E. (2014). The influence of coarse woody debris on soil carbon and nutrient pools 15 years after clearcut harvesting in black spruce—Dominated stands in northwestern Ontario, Canada. *Écoscience*, *21*(1), 11–20. https://doi.org/10.2980/21-1-3647

Yao, Y., Zhong, Z., Yang, X.-Q., & Huang, X. (2018). Seasonal variation of the North Pacific storm-track relationship with the Subarctic frontal zone intensity. *Dynamics of Atmospheres and Oceans*, *83*, 75–82. https://doi.org/10.1016/j.dynatmoce.2018.06.003

Yatskov, M. A., Harmon, M. E., Barrett, T. M., & Dobelbower, K. R. (2019). Carbon pools and biomass stores in the forests of Coastal Alaska: Uncertainty of estimates and impact of disturbance. *Forest Ecology and Management*, *434*, 303–317. https://doi.org/10.1016/j.foreco.2018.12.014